2006

PEPTIDE DEFORMYLASE: A MODELING STUDY OF THE ACTIVE SITES OF PLANTS AND BACTERIA AND THE DESIGN, SYNTHESIS, AND BIOLOGICAL ACTIVITY ANALYSIS OF PEPTIDE-BASED INHIBITORS

Jonathan C. Barnes
University of Kentucky, jcbch3@yahoo.com

ABSTRACT OF THESIS

PEPTIDE DEFORMYLASE: A MODELING STUDY OF THE ACTIVE SITES OF PLANTS AND BACTERIA AND THE DESIGN, SYNTHESIS, AND BIOLOGICAL ACTIVITY ANALYSIS OF PEPTIDE-BASED INHIBITORS

All nascent polypeptides synthesized in bacteria, mitochondria, or chloroplasts start with a *N*-formylmethionine. Peptide deformylase (PDF) is a mononuclear metal ion protein that is responsible for removing the *N*-formyl group of nascent proteins found in bacteria and chloroplasts in order for them to become mature proteins. It is possible, as seen from the literature with actinonin, to chelate the enzyme's metal ion and inhibit the function of protein production essentially resulting in death of the bacteria, or plant. This study examines the active site of *Arabidopsis thaliana* (*At*) types of PDF (*At*DEF1 and *At*DEF2, respectively) as well as bacterial DEF2 using sequence alignments and computational modeling. This work also investigates the biological efficacy of designing and synthesizing inhibitors that mimic actinonin or the D1 substrate that will halt, or severely retard, the activity of the PDF enzyme in vitro and in vivo. Through this research, we were able to determine specific residues that were conserved amongst the plant DEF2 sequences that were present less than 20% of the time in plant DEF1 and bacteria DEF2. This data allowed us to hypothesize plant DEF2's substrate specificity as well as a possible design that is selective towards plants and not bacteria. Also, based on preliminary results, the novel thiol-actinonin chimera that was synthesized showed inhibition activity of *At*DEF2 during in vitro enzyme assays.

KEYWORDS: Peptide deformylase, *N*-formylmethionine, DEF2, *Arabidopsis thaliana*, Actinonin.

MULTIMEDIA ELEMENTS USED: JPEG (.jpg), CHEMDRAW (.cdx), EXCEL (.xls)

Jonathan C. Barnes

December 18th 2006

PEPTIDE DEFORMYLASE: A MODELING STUDY OF THE ACTIVE SITES OF PLANTS AND BACTERIA AND THE DESIGN, SYNTHESIS, AND BIOLOGICAL ACTIVITY ANALYSIS OF PEPTIDE-BASED INHIBITORS

By

Jonathan Christopher Barnes

Dr. Robert B. Grossman
Director of Thesis

Dr. Robert B. Grossman
Director of Graduate Studies

December 18th 2006

RULES FOR THE USE OF THESES

Unpublished theses submitted for the Master's degree and deposited in the University of Kentucky Library are as a rule open for inspection, but are to be used only with due regard to the rights of the authors. Bibliographical references may be noted, but quotations or summaries of parts may be published only with the permission of the author, and the usual scholarly acknowledgements.

Extensive copying or publication of the thesis in whole or in part also requires the consent of the Dean of the Graduate School of the University of Kentucky.

A library that borrows this thesis for use by its patrons is expected to secure the signature of each user.

Name Date

THESIS

Jonathan Christopher Barnes

The Graduate School

University of Kentucky

2006

PEPTIDE DEFORMYLASE: A MODELING STUDY OF THE ACTIVE SITES OF PLANTS AND BACTERIA AND THE DESIGN, SYNTHESIS, AND BIOLOGICAL ACTIVITY ANALYSIS OF PEPTIDE-BASED INHIBITORS

THESIS

A thesis submitted in partial fulfillment of the
requirements for the degree of Master of Science in the
College of Arts and Sciences
at the University of Kentucky

By

Jonathan Christopher Barnes

Lexington, Kentucky

Director: Dr. Robert B. Grossman, Professor of Chemistry

Lexington, Kentucky

2006

ACKNOWLEDGEMENTS

This thesis represents the fruition of my research as a BS-MS student at the University of Kentucky. Firstly, I would like to specially thank Dr. Robert Grossman for his unwavering belief and support in my abilities to conduct said research. Through his knowledge, dedication, and passion of organic chemistry, I was able to achieve my many goals throughout this research project. Dr. Grossman's supervision and input was absolutely vital to any and all outcomes of this project. Secondly, I would like to thank Dr. Mark Williams, Dr. David Rodgers, Dr. Lynette Dirk, and Dr. Robert Houtz for all of their guidance and overall contribution to my knowledge accrued throughout this process. Without all of whom this collaborative project would have never been possible. Finally, I would like to thank all of my committee members: Dr. Grossman, Dr. Williams, Dr. Rodgers, and Dr. Arthur Cammers.

I also wish to express gratitude to my fellow lab mates over the years for all of their help and training. The list includes: Dr. Freddie Hughes, Dr. Roxana Ciochina, Dr. Razi Husseini, Suresh Jayasekara, Raghu Chamalla, and Uma Mallik.

TABLE OF CONTENTS

LIST OF TABLES

LIST OF FIGURES

LIST OF SCHEMES

LIST OF FILES

JCB_thesis.pdf ……2.14 MB

Chapter 1: Introduction to Peptide Deformylase (PDF)

1.1 Initial Discovery and Studies of PDF

Peptide Deformylase (PDF) was first investigated in the late 1960's by Jerry M. Adams at Harvard University. By incubating formyl-Met-Ala-Ser (fMAS) peptide with dialyzed extracts from *Escherichia coli* and *Bacillus stearothermophilus*, Adams observed, via electrophoresis experiments in conjunction with ninhydrin quantification methodology, that the formyl groups of formylmethionyl peptides were cleaved resulting in the methionyl peptides.[1] He entitled the enzyme peptide deformylase that was responsible for the activity observed. Adams went even further to show, by using homologues of fMAS, that there existed an enzyme activity that was responsible for the further cleavage of the methionine residue; aptly entitled methionine aminopeptidase (MAP).[1] Adams hypothesized that MAP was selective in the methionyl proteins it would cleave based on the residue that was adjacent to the aminoterminal methionine.

Many years later, in the mid 1980's, Fred Sherman, John Stewart, and Susumu Tsunasawa performed a study that supported Adams' hypothesis. They showed that MAP would only cleave the aminoterminal methionine if it were present adjacent to one of the following residues: alanine, cysteine, glycine, proline, serine, threonine, and valine.[2] In contrast, MAP would not cleave the terminal methionine if it were directly adjacent to the residues arginine, asparagine, aspartic acid, glutamine, glutamic acid, isoleucine, leucine, lysine, or methionine.[2] They suggested that the size of the adjacent residue's side chain had to have a radius of gyration of 1.29Å or less in order for the MAP enzyme to successfully complete the synthesis of the resultant protein.[2]

However, Adams' main efforts involved the study of PDF and not MAP. His attempts to stabilize the enzyme PDF were difficult at best due to what we now know is oxidation of the iron cation at the enzyme's center.[3] In his attempts to stabilize the enzyme (pH, buffer and ionic strengths, EDTA, etc.) he used a range of thiols that were commonly used for protein synthesis. The usage of the various thiols produced an interesting result as seen in (Table 1.1**)**.[1] Essentially, the thiols were in the concentration range of 0-6 mM in the extracts, which for some of the thiols was sufficient to reduce the

enzyme's activity to negligible percentages.[1] This loss in enzyme activity via the engagement of thiols will prove useful for inhibitor design, which is discussed later.

The basic biological function of the PDF enzyme, in regards to the line of steps post-translation, is to remove the formyl group that is placed on all plant protein sequences. This is done so the synthesized protein can be "marked" accordingly after the removal of the terminal methionine. The "marker" can be any number of post-translational modifications like hydroxylation, or methylation, etc. The "marker" is then recognized by other proteins that are responsible for the transportation of the mature protein to the appropriate location within the cell. Without this universal initiation step, the *N*-terminus formyl group on all proteins would remain, and the protein would be degraded and recycled resulting in overall plant death.

Table 1.1: Percent Activity of PDF When Incubated with Certain Thiols[1]

Thiol	Concentration (mM)	Percent Activity of an Undialyzed Extract
None	0.0	95.0
β-Mercaptoethanol	6.0	5.0
Reduced Glutathione	6.0	5.0
Cysteine	6.0	<2.0
Oxidized Glutathione	3.0	25.0

Further studies of the enzyme Peptide deformylase have shown it to be a mononuclear metal ion protein. In the early 1990's, the metal cation at the heart of PDF was believed to be Zn^{2+} based on structural similarities observed to metalloproteases found in the zinc metalloprotease family. However, the enzyme appeared to have a low activity of 0.8 U/mg against the fMAS substrate.[4,5] However, Dehua Pei's group at Ohio State University was able to increase this activity to 220 U/mg for the zinc-containing enzyme using bacterial overproduced purified enzyme preparations.[6] A few years later, during the mid-1990's, Groche and Wagner et al. were able to determine that PDF was actually an Fe^{2+} enzyme with a specific activity of 1200 U/mg and that Ni^{2+} also showed high activity figures relative to the iron-containing enzyme.[7,8,9] The purification was

accomplished for the labile iron-containing PDF by using catalse as a stabilizing agent against oxidation during the purification procedure.[7,8,9]

Studies by Meinnel and Blanquet have provided evidence that certain sequences relative to the PDF active site are conserved throughout the bacterial form of PDF.[10] In their study they aligned nine bacterial PDF sequences. Their original contention for zinc to be the metal cation at the core of the enzyme was based on the signature sequence HEXXH (histidine, glutamic acid, any amino acid, any amino acid, histidine) found near the active site, which is found in the zinc metalloprotease family.[10] They also noticed another conserved sequence of amino acids, EGCLS (glutamic acid, glycine, cysteine, leucine, serine) near the active site. A third and final conserved sequence was recognized also. That sequence was found to be GXGXAAXQ (glycine, any amino acid, glycine, any amino acid, alanine, alanine, any amino acid, and glutamine).[10] Through this study, and that of Becker and Wagner et al., it was gleaned that the two histidines in the HEXXH conserved sequence bind to the metal ion, as does the cysteine from the conserved sequence EGCLS and a water molecule.[10,11] Hence, the metal ion in the PDF enzyme is tetrahedrally coordinated. Similar instances of conserved sequences of residues near the active site are observed with plant *At*DEF1 and *At*DEF2 (*Arabidopsis thaliana* PDF types 1 and 2, respectively) and will be discussed in further detail later in the text.

1.2 Actinonin: The Gold Standard in PDF Inhibition

1.2.1 Initial Structural Constitution of Actinonin

Actinonin **1** (Figure 1.1) was initially isolated from a Malayan strain of *Actinomyces* by R. Green and R. Bhagwan Singh.[12] Green and Singh systematically screened soil and other materials to find microorganisms that possessed antibiotic properties. They found a new species of actinomycete that proved active against a number of bacterial strains. Gordon et al. were able to devise a procedure for the cultivation of the organism and for the isolation of the active ingredient, actinonin, in the early 1960's.[12] Upon testing actinonin against several Gram-positive and Gram-negative bacteria, Gordon and his colleagues observed the compound possessed great antibiotic properties.[13] They observed the melting point of actinonin to be 148° and the formula to

be $C_{19}H_{35}N_3O_5$ via compositional analysis and high resolution mass spectrometry.[13] The compositional analysis included extensive hydrolysis of actinonin using hydrochloric acid, derivative tests, and NMR and MS studies.

The results of the analysis yielded the conclusion that actinonin was comprised of D-pentylsuccinic acid, L-valine, L-prolinol, and hydroxylamine with the depletion of three water molecules.[13] This composition was intriguing because most polypeptide antibiotics known at the time were made of D-amino acid residues.[14] The structure of actinonin (Figure 1.1) contains only L-amino acid residues.

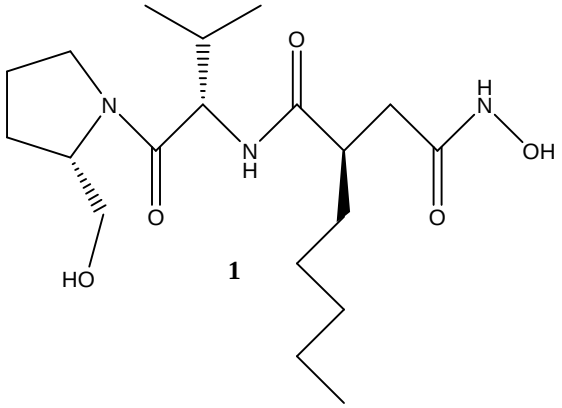

1

Figure 1.1: Structure of Actinonin 1.

1.2.2 Total Synthesis of Actinonin/Analogues via the Isomaleimide Methodology

Based on the constitution studies of actinonin discussed earlier, Anderson et al. were able to devise a synthesis involving the coupling of L-valyl-L-prolinol (**2**) and a derivative of pentylmaleic anhydride **3** (Scheme 1.1).[15]

Scheme 1.1: Coupling of L-valyl-L-prolinol (2) and Pentylmaleic Anhydride Derivative 3.

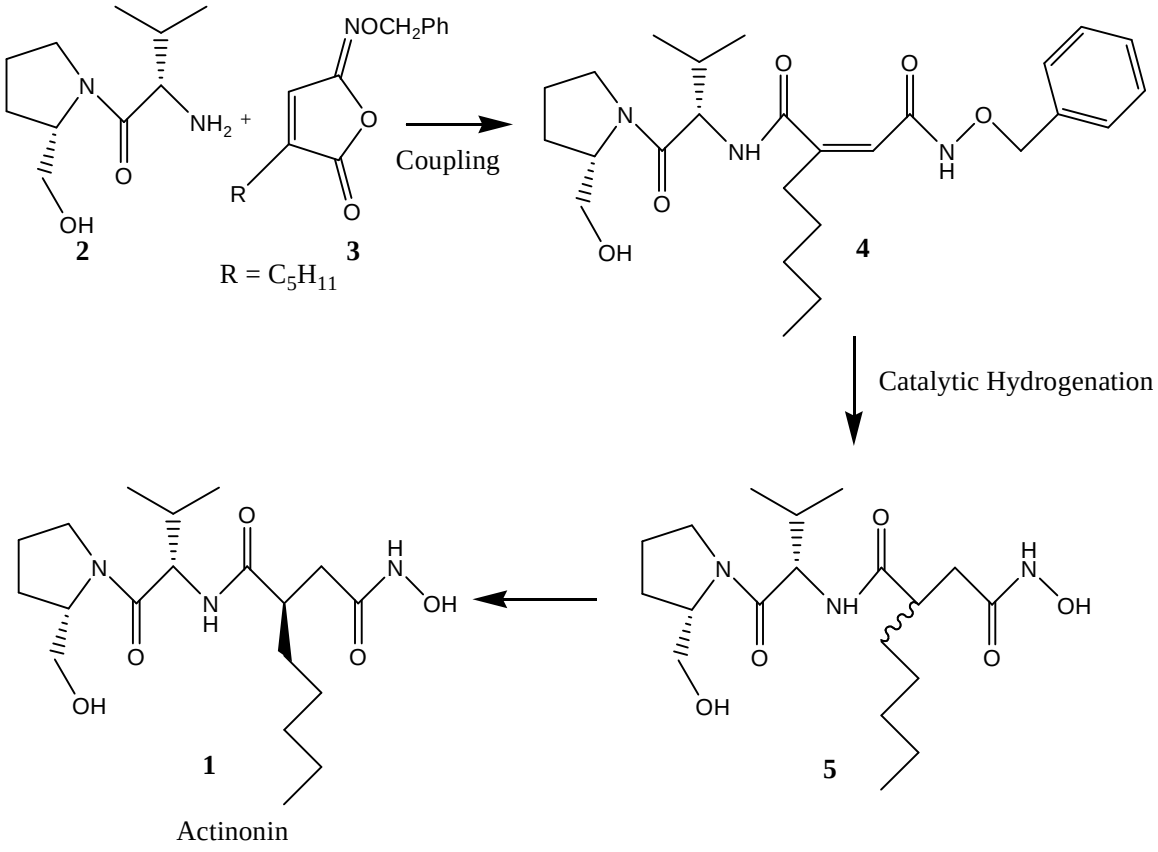

In order to synthesize **2**, Anderson et al. started with reduction of L-2-ethoxycarbonyl-5-pyrrolidone (**6)** via lithium aluminum hydride (LAH) in anhydrous ether followed by continuous extraction for 24 hrs to obtain L-prolinol (**7)**.[15] Then, **7** and the valine-derived ester **8** were coupled in ethyl acetate at room temperature to yield the dipeptide product **9**.[15] Finally, **9** was reduced to **2** via catalytic hydrogenation with 10% palladium-charcoal to form the carbamic acid intermediate **10** and subsequent thermal decarboxylation yielded **2** (Scheme 1.2).[15]

Scheme 1.2: Synthesis of L-Valyl-L-Prolinol (2).

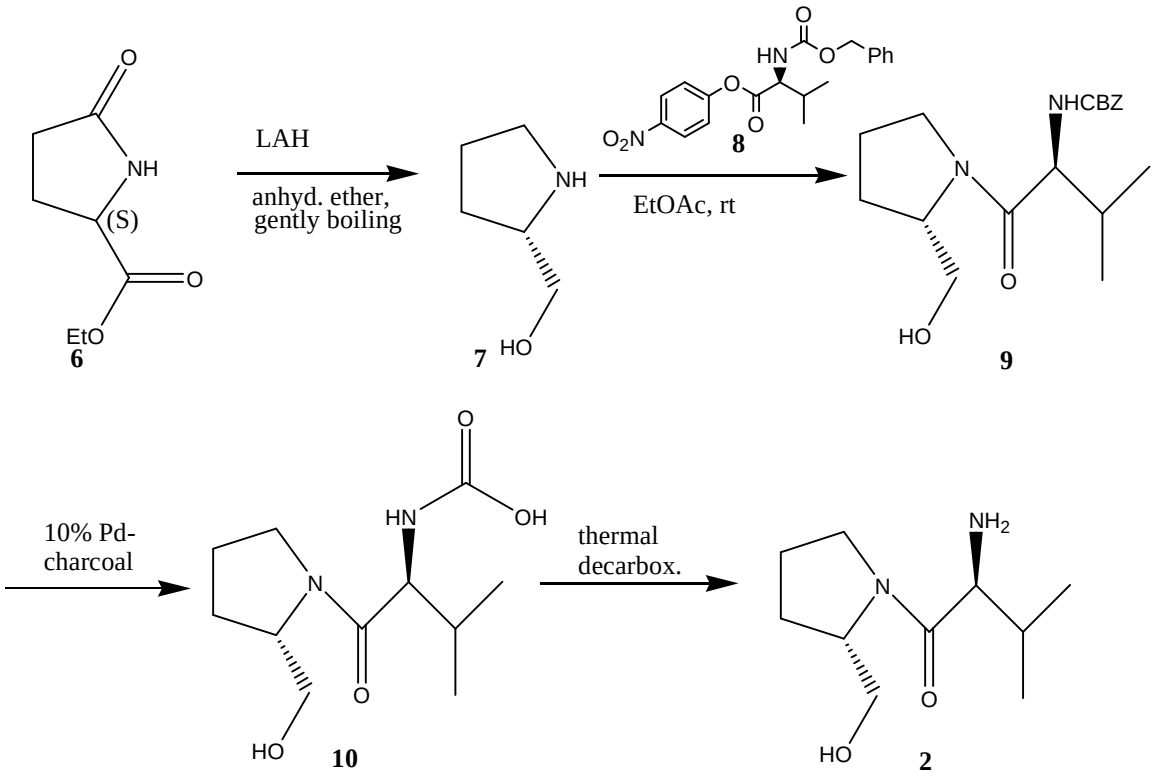

Initially, Anderson, et al., believed that the synthesis could be accomplished using pentylsuccinic anhydride **10** reacted with *O*-benzylhydroxylamine (**12**) to produce the pentylsuccinamic acid derivative **13** (Scheme 1.3).[15] They later decided to use pentylmaleic anhydride **11** to produce the pentylmaleamic acid derivative **14** instead because they believed there would be more selectivity for the carbonyl group which is remote from the alkyl substituent in **11** (Scheme 1.3).[15] However, by choosing the maleic anhydride route over the succinic anhydride route, they would have to eventually hydrogenate the double bond.

Scheme 1.3: Synthesis of Maleamic Acid 14: Pentylsuccinic Anhydride 10 and Pentylmaleic Anhydride 11 Reacted with O-benzylhydroxylamine (12) to give the Corresponding Acids 13 and 14, respectively. The arrow on **11** indicates the preferred carbonyl group by nucleophilic amines.

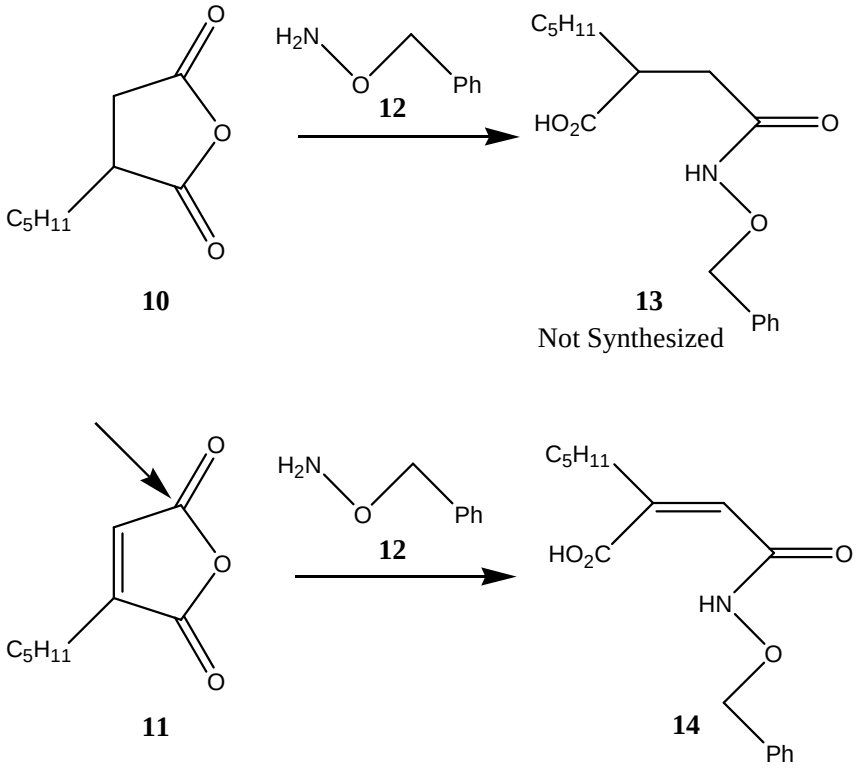

Next, Anderson et al. dehydrated **14** using *N*, *N*'-dicyclohexylcarbodiimide (DCC) to obtain the desired isomaleimide **3** and the maleimide **16** isomers (Scheme 1.4). The successful completion of these products was determined using ozonolysis reactions and identifying the resultant 2,4-dinitrophenylhydrazones.[15]

Scheme 1.4: Dehydration of 14 to Produce Isomaleimide 3 and Maleimide 16 Derivatives.

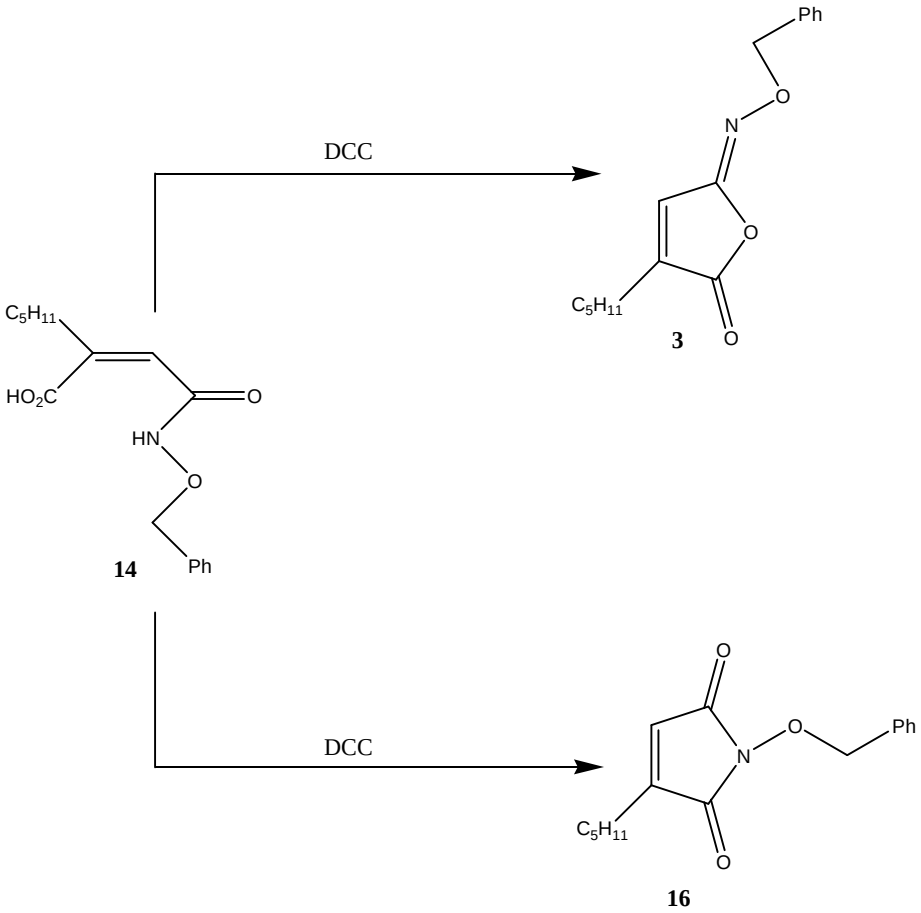

Next, Anderson et al. reacted **3** with **2** to produce *O*-benzyldidehydroactinonin (**4**) (Scheme 1.1).[15]. After catalytic hydrogenation of **4** and purification of the diastereomers of actinonin **5**, the antibiotic actinonin **1** was obtained.[15]

Scheme 1.1: Coupling of L-valyl-L-prolinol (2) and Pentylmaleic Anhydride Derivative 3.

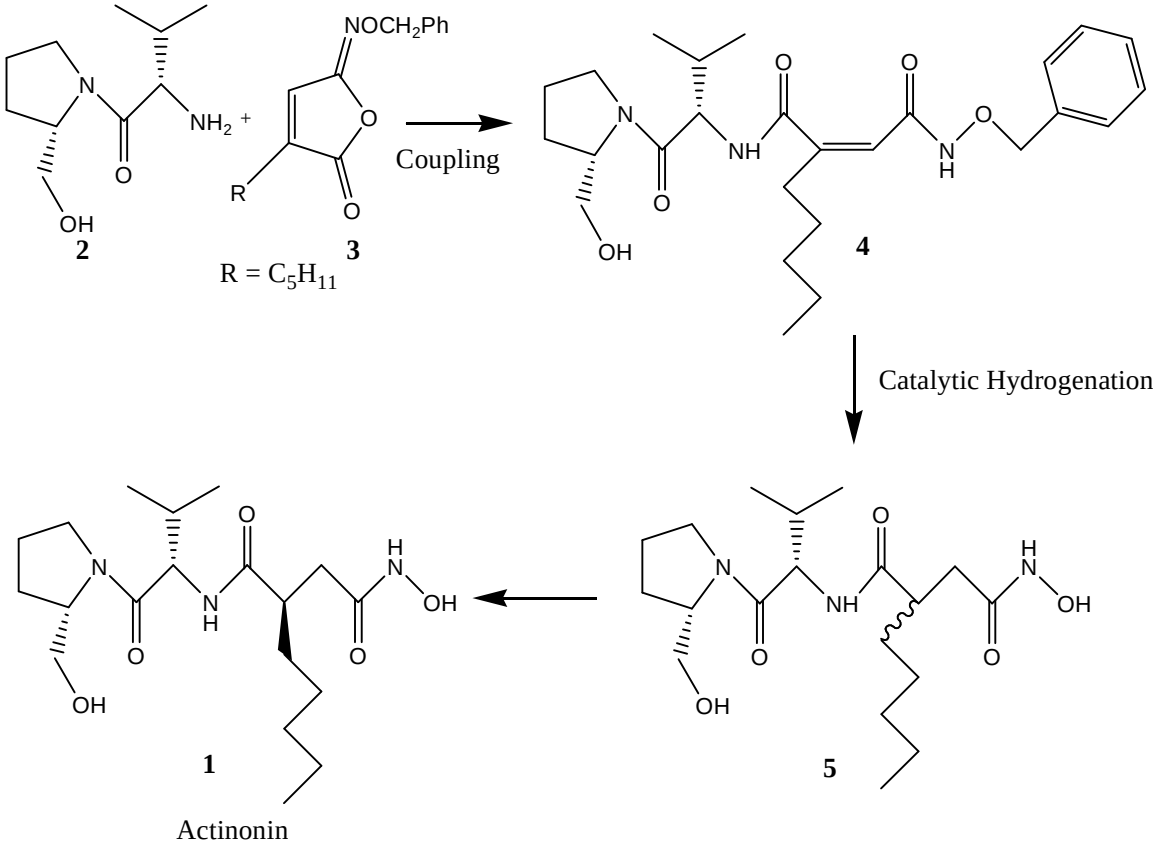

This isomaleimide methodology was applied to form analogues of actinonin. These analogues were made by replacing the L-prolinol, L-valine, or D-pentylsuccinic acid residues with pyrrolidine, alanine, or succinic acid residues, respectively, while keeping the hydroxamic acid chelating fragment constant.[15]

1.2.3 Survey of Other Methodologies Used for the Synthesis of Actinonin Analogues

During the initial studies of actinonin, it was observed that even though it showed antibiotic characteristics with various bacteria it also caused the fast appearance of

resistant strains to the compound.[16] With this in mind, Anderson, Devlin, et al., decided to synthesize analogues of actinonin in hopes of competing with the resistant strains.[16] The main similarity between all of these analogues is that they maintain the hydroxamic acid chelating group found in actinonin. The other residues found in the backbone of actinonin, such as the L-prolinol, L-valyl, and D-pentylsuccinic acid residues, are varied.

The various methods include the already discussed isomaleimide route[15], the anhydride-imide method[16], the mixed anhydride method[17], the anhydride-ester route[18], and the dicyclohexylcarbodiimide (DCC) coupling reactions[19]. Basically, all of the anhydride routes involve anhydro-derivative ring cleavage due to nucleophilic attack by an amido-amine.[19] Synthetically, the isomaleimide and anhydride-imide methodologies are useful because they lead to the side chain closest to the hydroxamic acid group (R_d, a pentyl hydrocarbon side chain in actinonin) having a β-position **17** relative to the hydroxamic acid residue (Figure 1.2).[18]

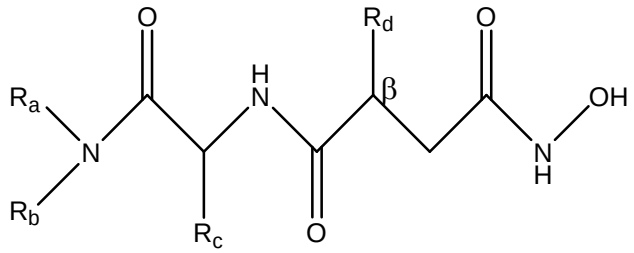

17

Figure 1.2: Actinonin Backbone; R_d is ß to the hydroxamic acid residue.[18]

The anhydride-ester methodology is synthetically useful because it affords an α-relation **18** of the R_d side chain to the hydroxamic acid residue to produce other actinonin analogues (Figure 1.3).[18]

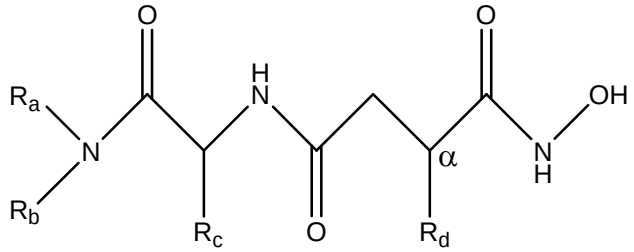

18

Figure 1.3: Actinonin Backbone; Rd is α to the hydroxamic acid residue.[18]

The DCC coupling reactions are of significant importance for three reasons. First, this was the first ever reported usage of the reagent DCC to form amide bonds from amino-amides and esters of dicarboxylic acids.[19] Secondly, this synthetic route allowed for the amide bonds to be formed without having to cleave a ring via nucleophilic attack on cyclic anhydro-derivatives, as was the case with the isomaleimide, anhydride-imide, and anhydride-ester methodologies.[19] Finally, this coupling methodology proved highly effective in the synthesis of my chimera of actinonin and an existing sulfhydryl, which will be discussed further in Chapter 3.

1.2.4 Actinonin's Inhibitory Effect on Bacterial PDFs

Due to the increase in pathogenic bacteria that are resistant to current antibiotics, a search has evolved over the last several years to find a new, selective target common to all bacteria that doesn't affect mammals.[20] Peptide deformylase serves as an ideal target due to its ubiquity throughout the bacterial spectrum, its importance to the microorganism, and its low functionality in mammalian cells. In 2000, Chen et al. showed that the naturally occurring actinonin **1** served as a potent, reversibly specific inhibitor of the enzyme peptide deformylase.[20] Also, at the time of Chen's publication, there were no known inhibitors reported that inhibited protein modification after translation.[20]

In order to prove actinonin's specificity for the enzyme peptide deformylase, Chen et al. started with dose-dependent studies comparing the level of actinonin concentration vs. PDF activity. They discovered that for Ni-PDF, the IC_{50} values (50% inhibitory concentration) approached approximately 50% of the concentration of the enzyme used, suggesting that actinonin is bound very tightly by PDF and the IC_{50} changed when the enzyme concentration changed.[20]

To further confirm actinonin's specificity for PDF, Chen et al. used the arabinose promoter P_{BAD}-*def* of *E. coli tolC* to control the level of expression of deformylase by regulating the amount of inducer (arabinose) present.[20] The more arabinose present, the more expression of the deformylase gene, and vice versa. When the arabinose level was made low, the *def* genes became underexpressed and the PDF enzyme became more vulnerable to inhibitors specific to PDF.[20] Conversely, when the gene was

overexpressed, one would expect an increase in the minimum inhibitory concentration (MIC) of the inhibitor.[20] Over a range of arabinose levels, only actinonin showed a relationship between the arabinose inducer concentration and the MIC.[20] To further support the claim of specificity of actinonin for PDF, the other inhibitors used (fosfomycin and ciprofloxacin) showed no relationship to the inducer concentration levels and maintained the same MIC throughout.[20] Even after altering another P_{BAD}-*def* gene that was not dependent on the arabinose concentration, there existed a similar relationship between the two P_{BAD}-*def* strains for the enzyme's susceptibility to actinonin.[20] This data supports the theory that actinonin is PDF specific.

In using Zn-PDF, Chen et al. discovered that the IC_{50} values were the same regardless of the incubation time, which ranged from 10 minutes to 100 minutes.[20] This further supports that actinonin is a fast, tight binding inhibitor. Again using the Zn-PDF, no PDF activity was observed in the presence of actinonin. After dialysis of the samples for 48 hrs, which removes any free actinonin, the PDF activity was restored to that of the control sample, showing actinonin is a reversible inhibitor. [20]

Chen et al. concluded that actinonin was a competitive, reversible, tight-binding inhibitor with a chelating hydroxamic acid group. Based on their results, and modeling studies not yet mentioned, they suggested that analogues of actinonin would be the best possible route to new antibiotics.[20] Not only was the production of analogues important because of the emergence of resistant strains, but also because their in vivo studies with actinonin showed a lack of potency. This lack of potency was later shown by Williams et al. to be due to the metabolic reduction and hydrolysis of the hydroxamate group.[26]

1.3 Actinonin: Chloroplast-Localized Plant PDF Inhibition

1.3.1 Eukaryotic Homologues: PDF in *Arabidopsis thaliana*

Hanson in 2000[21] hypothesized the importance of the enzyme peptide deformylase in plant plastids. Williams and Houtz in 2000[22, 23] hypothesized that the enzyme peptide deformylase would also play a vital role in protein production in plants, as had been the case for bacteria. Williams et al. [22] identified two types of PDF enzymes in plants that were essentially eukaryotic homologues of the more familiar bacterial (prokaryotic) deformylase. Using bacterially expressed *Arabidopsis thaliana* (*At*)

deformylases, Dirk et al. [23] compared the activity of the two plant versions of PDF, *At*DEF1 and *At*DEF2, by doing in vitro enzyme assays, in vivo studies involving the imbibing of Arabidopsis seeds, and direct topical application to leaves of *Arabidopsis* plants.

The in vitro enzyme assays consisted of a buffer solution containing bacterially processed *At*DEF2, actinonin, and an *N*-formyl-Met-Leu-ρ-NA substrate. The cleavage of the formyl group on the substrate caused the release of the para-nitroaniline group, which was spectrophotometrically observed at 405 nm. The assays of *At*DEF1 and *At*DEF2 with varying concentrations of actinonin showed comparable inhibitory results to that of the bacterial PDF-actinonin analyses.[23] For example, the IC_{50} for *At*DEF2 was a concentration slightly less than 100 nM of actinonin, while the concentration to decrease the enzyme's activity to virtually zero was 300 nM of actinonin.[23] Due to enzyme activity detection limitations, a higher concentration of *At*DEF1 was needed relative to *At*DEF2, which subsequently led to the results indicating an almost 2-fold weaker binding affinity between actinonin and *At*DEF1.[23]

The in vivo seed germination tests of *Arabidopsis* required the concoction of an agar medium with actinonin from which the seeds would derive the proper nutrients and uptake the inhibitor.[23] Varying concentrations of actinonin were used to properly analyze the inhibition of growth over the course of a week. The seeds that were grown from a medium containing no actinonin served as the controls, while concentrations of 0.81, 1.6, and 3.2 mM of actinonin served as the variables (Figure 1.4).[23] After 5 days, the actinonin concentration of 0.81 mM allowed normal cotyledon expansion from the *Arabidopsis* seeds, but there was no green color due to the lack of chloroplast production. Actinonin concentration at 1.6 mM hindered the spread of the cotyledons. Finally, the actinonin at 3.2 mM allowed only a slight emergence of the radicale and nothing further.

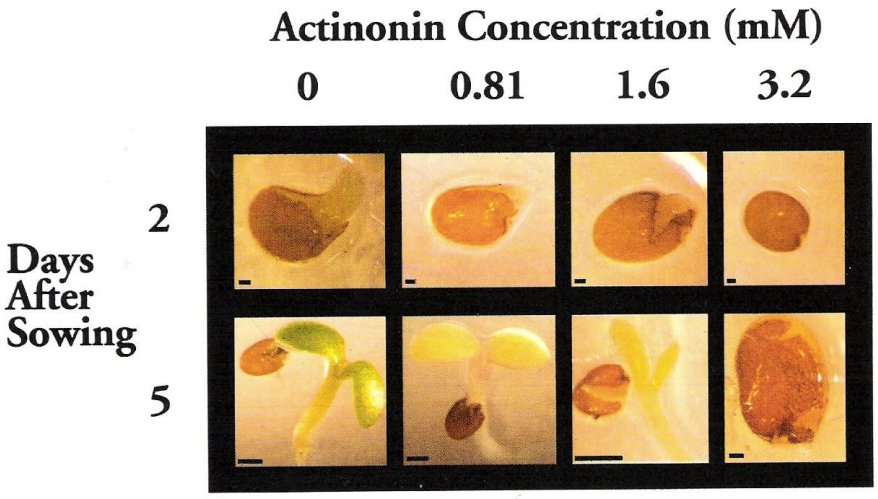

Figure 1.4: Actinonin treatment of *Arabidopsis*.[23]

Direct topical application of actinonin/detergent aqueous solutions to the leaves of Arabidopsis plants induced a retardation of growth and slow bleaching.[23] After a week of applications, the size and rate of growth of treated leaves was substantially inhibited, and loss of color, or bleaching, was observed.

1.3.1.1 D1 Specificity of PDF in *Arabidopsis thaliana*

Using peptide mimics of certain chloroplast-translated proteins, Dirk et al. in 2002[24] investigated *At*DEF2's substrate specificity based on enzymatic assay analysis and establishing kinetic rates for each mimic to determine adjacent residue effects. One of the more important peptide mimics that was studied was based on the D1 protein. The D1 protein is part of the photosystem II (PS-II) reaction center located in the thylakoid membrane, so any inhibition of the *At*DEF2 enzyme would interfere with the complete processing of the D1 protein and hence affect the outcome of the absolutely vital PS-II process.[24] It turns out that the D1 substrate mimic had the highest enzymatic activity recorded of all the mimics studied, indicating the *At*DEF2 enzyme's preference for this particular sequence. For the enzyme assays, *At*DEF2 was mixed with various chloroplast peptide analogues, and, using a spectrophotometer at a wavelength of 340 nm, the amount of NADH was observed. The more NADH present, the more processed a particular peptide mimic; hence a higher affinity of the substrate to bind to the PDF enzyme.

1.3.2 PDF Inhibition in *Nicotiana tabacum* and Reduction of D1 Protein

Apparently tobacco plants are not as susceptible to actinonin as are *Arabidopsis* and pea plants. At inhibitor concentrations where pea and *Arabidopsis* plants would bleach and die, the tobacco plants showed only stunting and some bleaching.[25] A study performed by Hou et al. in 2004[25] showed that by monitoring the quantum efficiency of chlorophyll fluorescence in plants, one is able to ascertain the effect of actinonin on photosystem II (PS-II) activity. It was observed that after five days of painting of the tobacco plant leaves, the PS-II activity had virtually ceased, but the plants did not bleach as did the pea and *Arabidopsis* plants..[25] The decrease in PS-II activity was attributed to a decrease in the level of D1 protein and hence the subsequent cessation of PS-II function. By not processing the *N*-formyl methionine portion of the D1 protein, one is able to block the production of the high-demand protein monomer, which is responsible for the reassembly of any disassembled PS-II complexes, thereby causing the death of the plant due to a lack of photosynthetic production.[25]

1.4 The Metabolism of Actinonin

Because actinonin **1** is capable of inhibiting PDF in many different types of plants (as evidenced by in vitro enzyme assays) and different types of plant seeds (as evidenced by in vivo seed germination tests), it was hoped that it could be used as a broad-spectrum herbicide.[26] This hope, however, turned out to be empty, due to the reduction and hydrolysis of the hydroxamate group to the resultant carboxylic acid **20** and amide **19** seen during in vivo plant studies and in vitro microsomal fraction analysis (Scheme 1.5).[26] According to Hou, et al.[26] tobacco plants are capable of absorbing and metabolizing all but 17% of the initially applied actinonin after 48 hours. They were able to isolate the two metabolites via reverse-phase HPLC and determine their formula based on mass spectrometric experiments (Figure 1.5).[26] They tested the metabolites' inhibition activity and showed they had relatively little effect on the DEF2 enzyme when compared to unmetabolized actinonin.[26] It is this effect that makes the search for nonmetabolyzable analogues of actinonin of considerable interest.

Scheme 1.5: In Vivo Reduction and Hydrolysis of Actinonin in Plants.

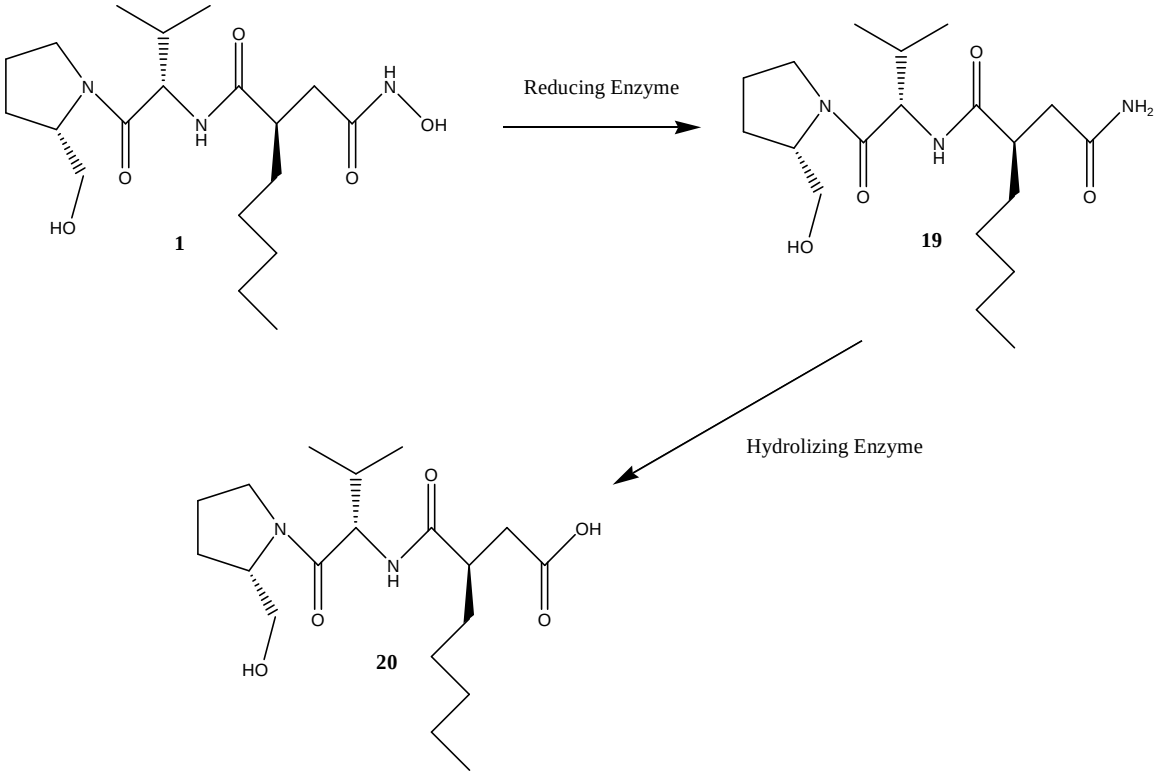

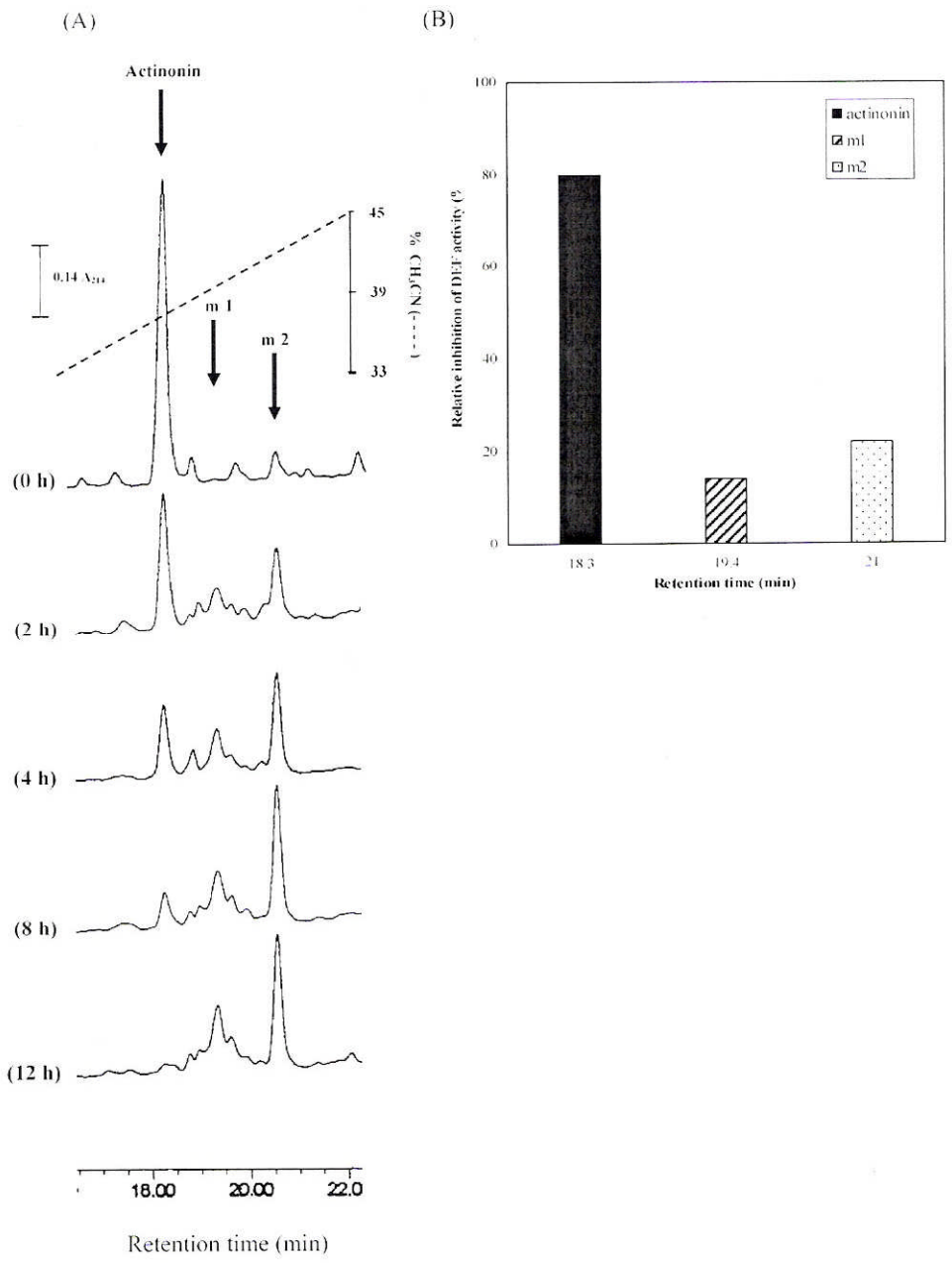

Figure 1.5: Reverse-Phase HPLC fractionation of actinonin after incubation with tobacco microsomes.[26] (A) Actinonin (40 μM) was incubated with tobacco root microsomal proteins and aliquots were removed at each time point and analyzed by HPLC. (B) The actinonin peak at 0 h and the m1 and m2 peaks from 12 h were collected, lyophilized, and reconstituted to volumes equal to those injected on the HPLC.

1.5 Survey of Various Types of PDF Inhibitor Designs

Due to the reduction and hydrolysis of the inhibitor actinonin **1** discussed in section 1.4 above, a new design is required where the inhibitor will not only fit well in PDF enzyme active sites and perform well during in vitro assays, but be resistant to breakdown in vivo. Three main types of inhibitors have been designed. The first are the analogues of the actinonin molecule retaining the hydroxamic acid group but with altered side chains (see sections 1.2.2 and 1.2.3).[16-19, 20, 27-30] Then there are the thiols, with sulfhydryls as the chelating group, and using different backbones from that seen in actinonin.[31-33] Finally, came attempts at solving the reduction and hydrolysis issues. In the third class, the hydroxamate chelating group is rearranged. This is done by reversing the location of the nitrogen and the *N*-hydroxyl group to the opposite side of the carbonyl, creating an aldehyde.[34,35] These compounds are discussed later in the text.

1.5.1 Linear Thiol PDF Inhibitor Designs

Huntington et al. in 2000[32] designed the first series of peptide-based thiols to serve as inhibitors of recombinant PDF from *E. coli* and *B. subtilis* (Scheme 1.6). They were able to obtain, via in vitro enzyme assays, K_I values, which reflected the potency of each inhibitor against PDF. Their best K_I value reported was for one of the thiol inhibitors, **29b,** with a potency of 19 $^{+}$/- 1 nM. The published synthesis combined an acetyl-protected thiol-acid **25** and a *p*-nitroaniline amine **27a-c**, to give the final thiol inhibitor (**29a-h**) after deprotection (scheme 1.6).[32]

Scheme 1.6: Pei's Synthesis of Peptide-Based Thiol Inhibitors[32]

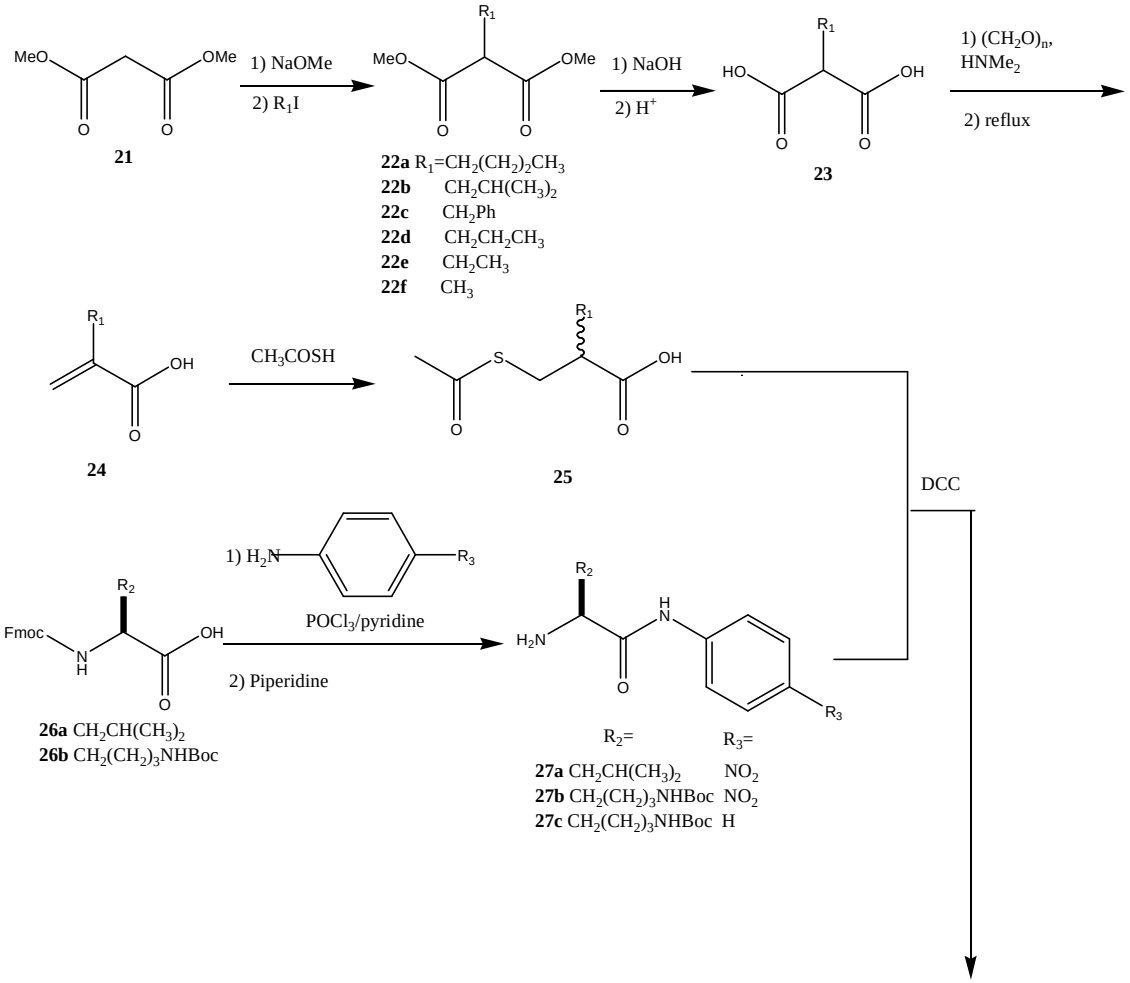

1.5.2 Reverse Hydroxamate Macrocyclic PDF Inhibitor Designs

The macrocyclic ring in the reverse hydroxamate compounds have been shown to reduce the proteolytic effect experienced in the cell media and increase the selectivity of peptide-based inhibitors.[36, 37] Using compound BB-3497's **30** (Figure 1.6) backbone, it is believed that the macrocyclic connection can be made between the P_1 and P_3 side chains, which causes an increase in active site binding.[34] Hu, et al., in 2003 set out to construct a macrocyclic reverse hydroxamate peptide-mimetic inhibitor **44** in hopes of solving the aforementioned hydrolysis and stability issues associated with actinonin (Schemes 1.7 and 1.8).[34, 36]

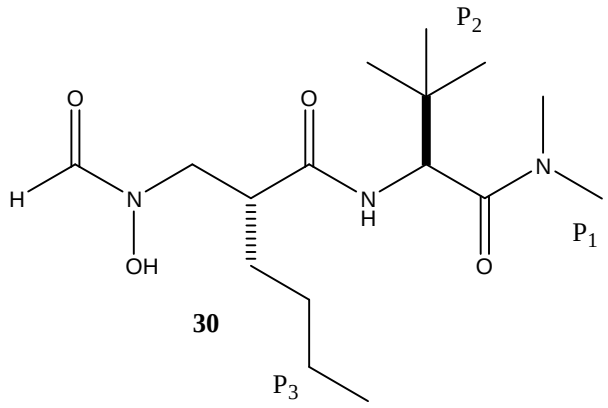

Figure 1.6: Structure of BB-3497 30. The $P_{1\text{-}3}$ notations indicate the three common positions of side chains relative to one another and the chelating group.

Formation of the first precursor **38** of the synthesis[34] (Scheme 1.7) involved starting with a simple commercial acid **31** and attaching a chiral auxiliary **32** in order to set the stereochemistry of the α-ethyl alcohol side chain in compound **34**. From there, the chiral auxiliary is cleaved and the acid is replaced with O-Benzylamine to form compound **35**. Next, a Mitsunobu reaction[34] is carried out to form the 4-membered lactam **36**, which is reopened **37**, and the amine is then protected with a formyl group to give the first precursor **38**.

The second precursor **41** and final coupling (Scheme 1.8) started with taking a simple, commercially available alcohol **39** and converting it to the primary amine **40**. Next, the primary amine **40** was combined with a commercially available leucine amino acid to form the second precursor **41**. Then, the second precursor **41** was coupled with the first precursor **38** to give the diene **42**. From the diene **42**, Grubbs' catalyst was used

to do an olefin metathesis reaction to close the ring to give the initial macrocyclic alkene **43**. Finally, the macrocyclic alkene **43** was debenzylated and reduced to give the final macrocyclic inhibitor **44**. [34]

Scheme 1.7: Synthesis of the First Coupling Precursor 38 of Compound 44.

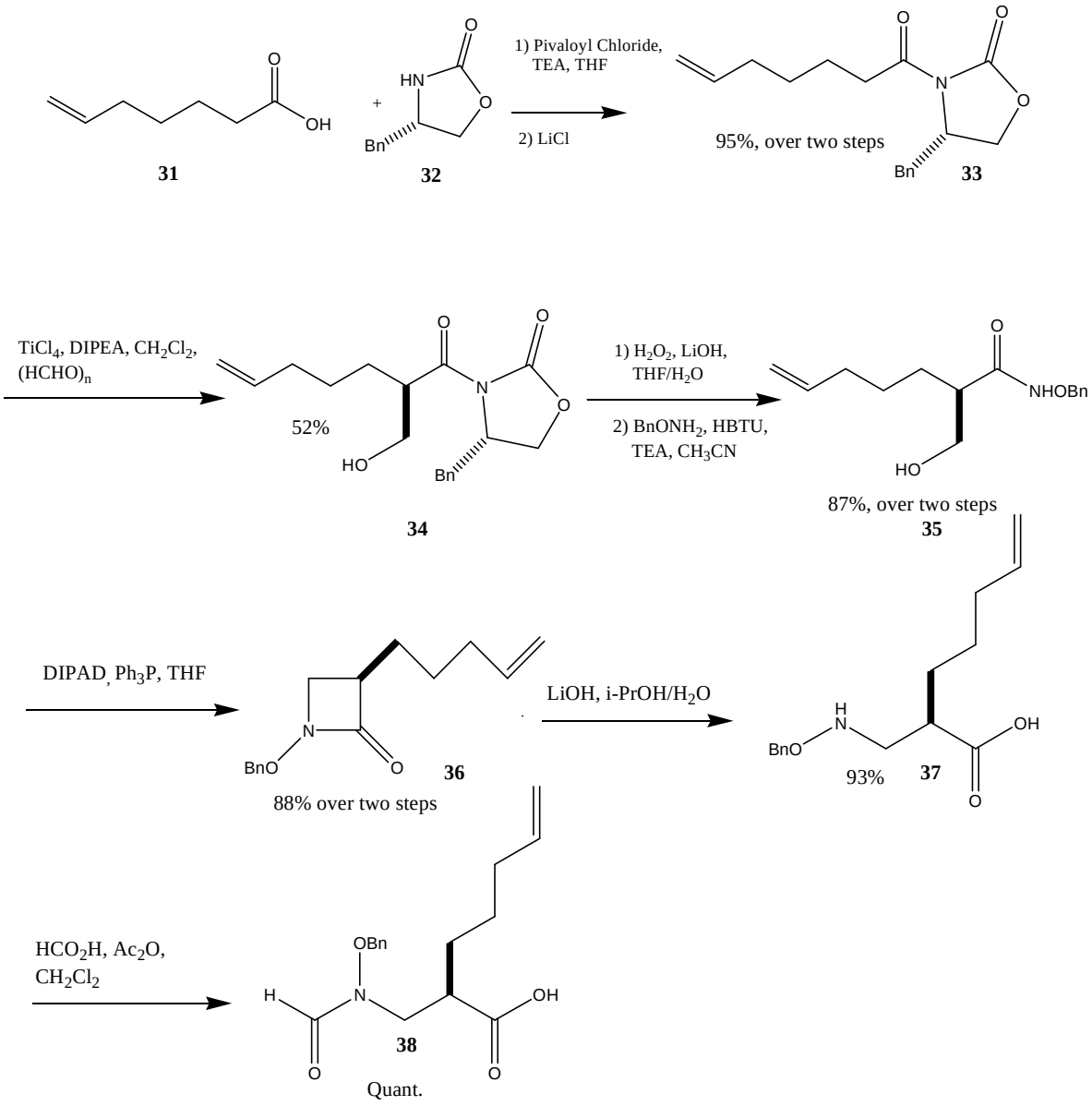

Scheme 1.8: Synthesis of the Second Coupling Precursor 41 and Final Coupling to Produce Compound 44.

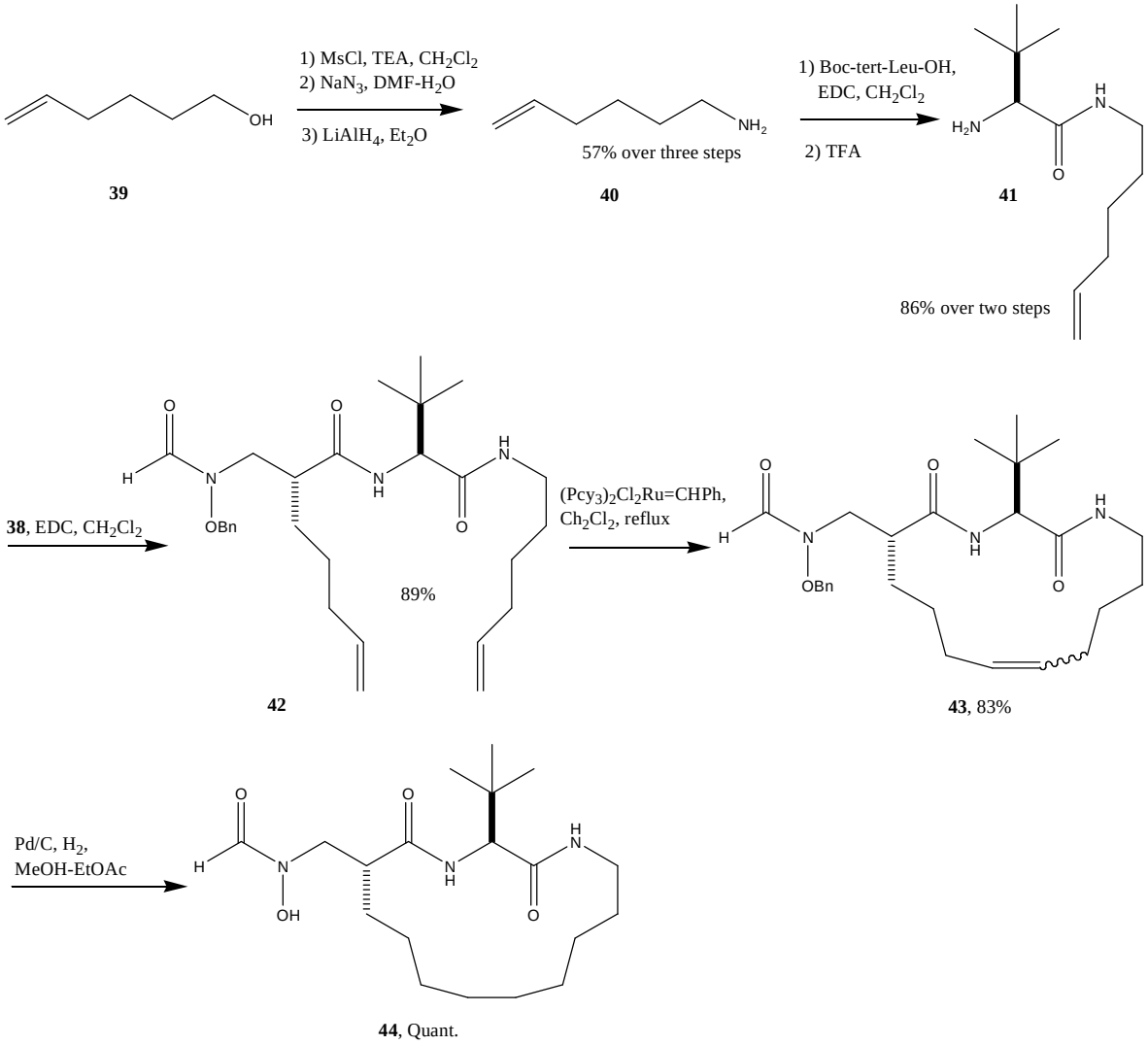

39 **40** **41** **42** **43**, 83% **44**, Quant.

Compound **44**'s potency was tested in a dehydrogenase enzyme assay with Co(II)-PDF (*E. coli*).[6,38] The result was a K_I constant of 0.67 $^{+}/_{-}$ 0.2 nM. This data shows that compound **44** is more than 10-fold more potent than the BB-3497 inhibitor (IC_{50} = 7 nM) it mimicked.[34, 39]

Hu et al. in 2004[35] went even further with their studies of the macrocyclic inhibitors by experimenting with the ring size. Through synthetic analogue studies, Hu et al. were able to find that the optimal ring size was 15-17-membered. Also, compared to the linear peptides of similar backbone, the macrocyclic inhibitors showed an

approximate 20-fold increase in potency, suffered less proteolytic hydrolysis, and had a higher selectivity for deformylase over other enzymes.[35] The potency of the inhibitors was very high, with K_I* constants in the 0.22-36 nM range when performing Aeromonas aminopeptidase (AAP) assays, and K_I constants in the 11-2100 nM range when performing dipeptidyl peptidase I (DPPI) assays, with *E. coli* PDF as the initiater. They also determined the new macrocyclic inhibitors to be slow-binding, as opposed to the linear counterparts, which bind quickly.[35] With the advent of these new macrocyclic inhibitors, and taking into account their high potency, the future for the design of inhibitors seems to prefer this type of scaffolding. For the purposes of plant PDF inhibition, and especially concerning the more important case of the degradative enzymes in vivo, the success of such inhibitors remains untested.

1.6 Project Agenda: Computational-Biological Analysis/Synthesis and Purification

Due to the integral function of the cleaving of the *N*-formyl group from nascent proteins post-translation, peptide deformylase is a good target for the development of antimicrobials and herbicides. The two biggest problems for this development involve the cross-over that could possibly be experienced when designing an inhibitor for plants that might also inhibit bacteria as well, and the search for a peptide-based inhibitor that can fit specifically into the PDF active site, but that can also survive the degradative enzymes found during in vivo studies.

With the first problem in mind, my collaborative research group proposed an analysis of the three main types of peptide deformylase: bacterial DEF2, plant DEF2, and plant DEF1 using computational modeling and alignment software to try to discern between the bacterial DEF2 and the plant DEF's. If there exists a difference in the active sites of the bacterial PDF and the plant PDFs, then one might be able to specifically design an inhibitor that can knock out plant PDFs and not the bacterial PDF. This would allow development of a new herbicide that does not adversely affect soil microorganisms.

Overcoming the second problem of interest was hypothesized to be possible if we could design a novel inhibitor that uses the exact backbone skeleton of actinonin up to the P_1 side chain and then replace the hydroxamate chelating group with a sulfhydryl group.

By doing this, it was believed the inhibitor would not undergo reduction and hydrolysis in vivo and at the same time be tightly bound in the active site of PDF because of the great in vitro success of actinonin observed in earlier studies. This hypothesis was tested after the synthesis and isolation of a novel thiol-actinonin inhibitor by performing in vitro enzyme assays, in vivo seed germination analyses, and in vivo topical leaf-painting experiments. The results showed the chimera to be an inhibitor of *At*DEF2 that was ten times less potent than actinonin (50 nM for actinonin and ~5000 nM for the chimera). Further studies are necessary in regards to the seed germination tests and the leaf painting experiments due to the material used at the time being crude.

Chapter 2: Computational Modeling/Analysis of Three Types of PDF Active Sites

2.1 Ligand Interaction Mapping

To begin this project, we wanted to answer the two questions concerning the comparison of plant DEF2 to both plant DEF1 AND bacterial DEF2. The first question was why does plant DEF2 prefer certain protein sequences over others, while plant DEF1 showed no great selectivity for any of the protein sequences?[24] In addition to the higher selectivity, plant DEF2 showed a 100-fold higher activity than plant DEF1.[24] The second question was are there enough differences in the active site residues between the bacterial forms of PDF and the plant forms of PDF? To answer these questions, we started by compiling a list of interacting ligands of *At*DEF2 using the protein data bank and its PDBSUM utilities.[40] Once a master list of interacting residues was constructed, we could map those particular interacting residues onto the coordinate file of our own crystal structure of *At*DEF2 obtained by Dr. Rodgers (Figure 2.1). The blue region shown in Figure 2.1 represents the residues in *At*DEF2 that interacted with the ligands found in the database.

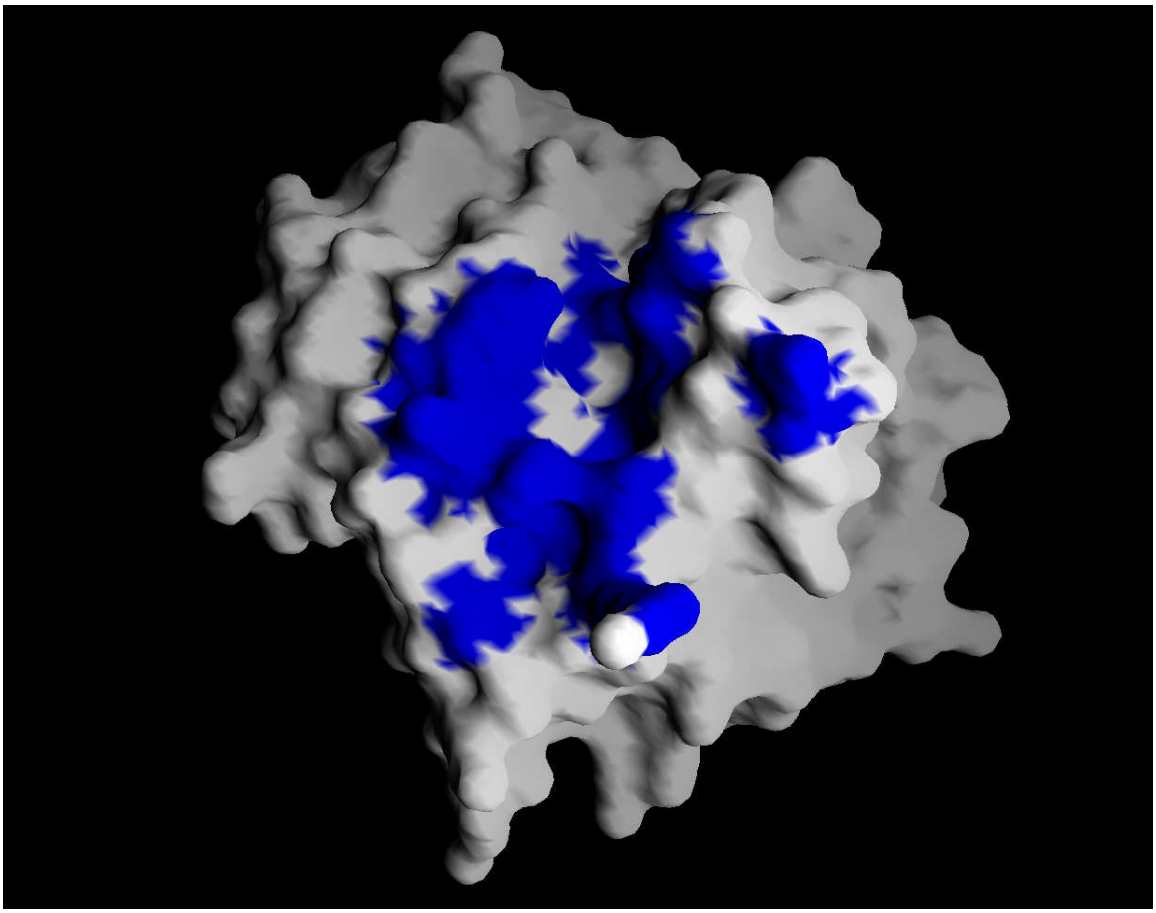

Figure 2.1: Interacting Residues Mapped on *At*DEF2. The crystal structure was obtained by Dr. Rodgers. The blue represents the region of general activity based on the database of ligands and their specific residue interactions.

2.2 Residue Conservation of the Three Types of PDF

With a general idea of the enzyme's active site now in hand, the next step was to identify how many of the residues are conserved. The following alignments of the three most highly conserved motifs near the active site were performed by Dr. Lynnette Dirk. The first step in conservational analysis involves performing a technique, known as BLAST (Basic Local Alignment Search Tool), on the chloroplast length peptide deformylase protein DNA sequence.[43] This was done so that the sequence could be compared to other sequences in the database and a statistical representation could identify regions of similarity. Next, the DNA sequences were translated into protein sequences, and a TargetP prediction was performed .[44] This prediction identifies the location of the N-terminus of the protein sequence for the mature length of the protein. Once the

location was found, the protein sequence was shortened to isolate that region. After duplicates and erroneous portions were removed, the remaining protein sequence motifs were then aligned using CLUSTAL W.[45] Finally, the sequences were counted at each residue position to see what residue each had and if it matched the *At*DEF2 sequence. They all were tallied into the three main motifs of the active site. The definition of conservation we decided to use was 50% or higher. This meant that at least 50% of the residues of the other sequences found in the database matched our *At*DEF2 residues. This alignment approach was performed for the *At*DEF1 and *Ecoli*DEF2 sequences as well. This conservational analysis would provide an insight into the more conserved, or more common, residues found in all plantDEF2's, plantDEF1's, and bacteriaDEF2's, respectively.

2.2.1 Conservation for *At*DEF2

The conservation discussed above was mapped to the enzyme *At*DEF2 (Figure 2.2). The blue color in Figure 2.2 represents the conserved residues and the violet color represents the non-conserved residues. Figure 2.3 represents a ribbons view of the three conserved motifs of *At*DEF2 as well.

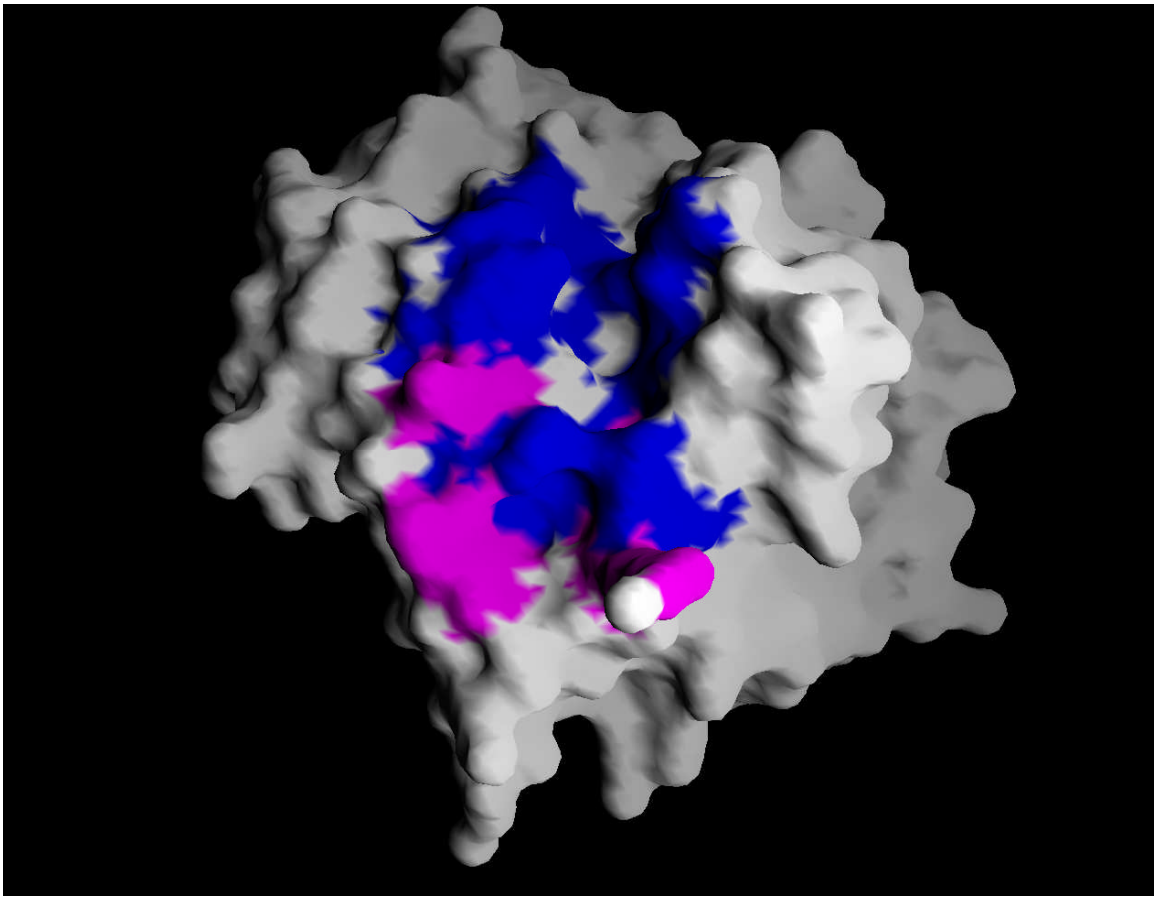

Figure 2.2: Conserved residues for *At*DEF2. The conserved residues are in blue and the non-conserved residues are in violet. The blue shading gives a more specific idea of the active site relative to the general interacting residues shown in Figure 2.1.

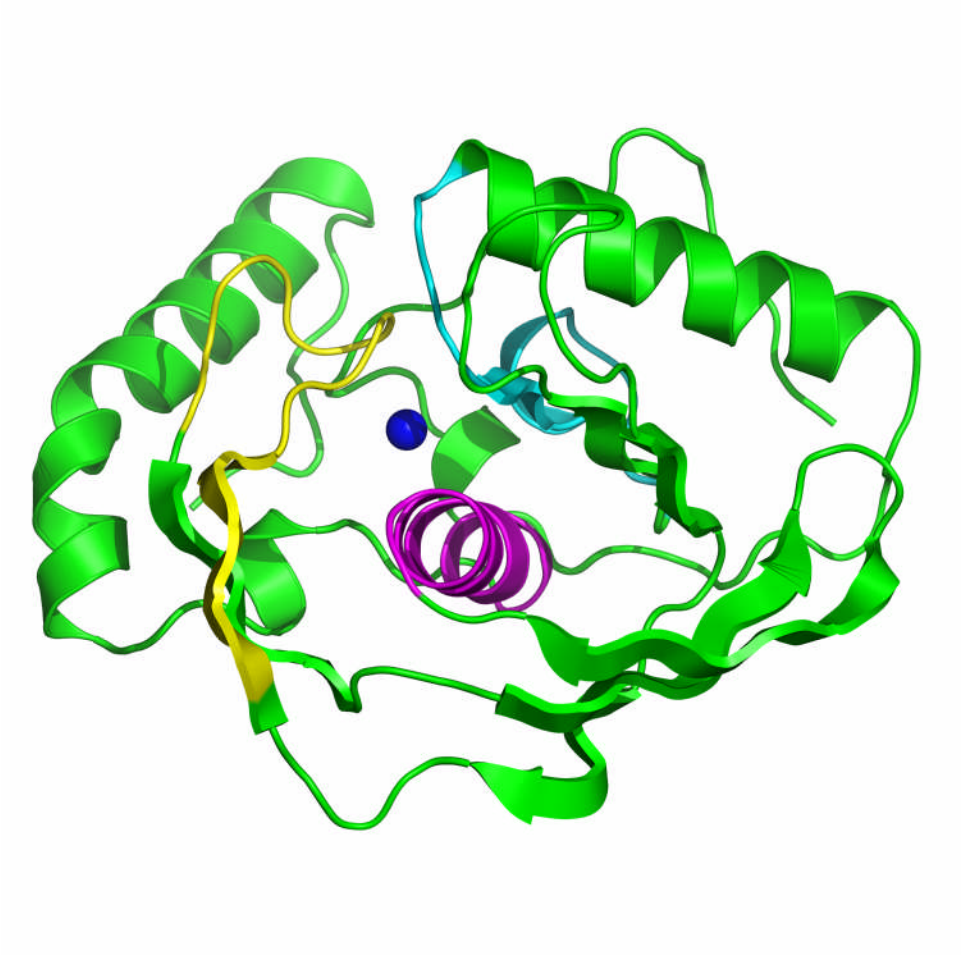

Figure 2.3: Ribbons view of the three conserved motifs of *At*DEF2. The yellow, purple, and blue ribbons represent the three motifs of the active site and the blue ball represents the enzyme's central metal.

2.2.2 Conservation for *At*DEF1

The conserved residues from the alignment studies discussed above were mapped onto an *At*DEF1 enzyme from the protein data base (Figure 2.4).[42] The blue again stands for conserved residues, while the non-conserved residues are in violet, which cannot be seen because they are on the opposite side of the enzyme.

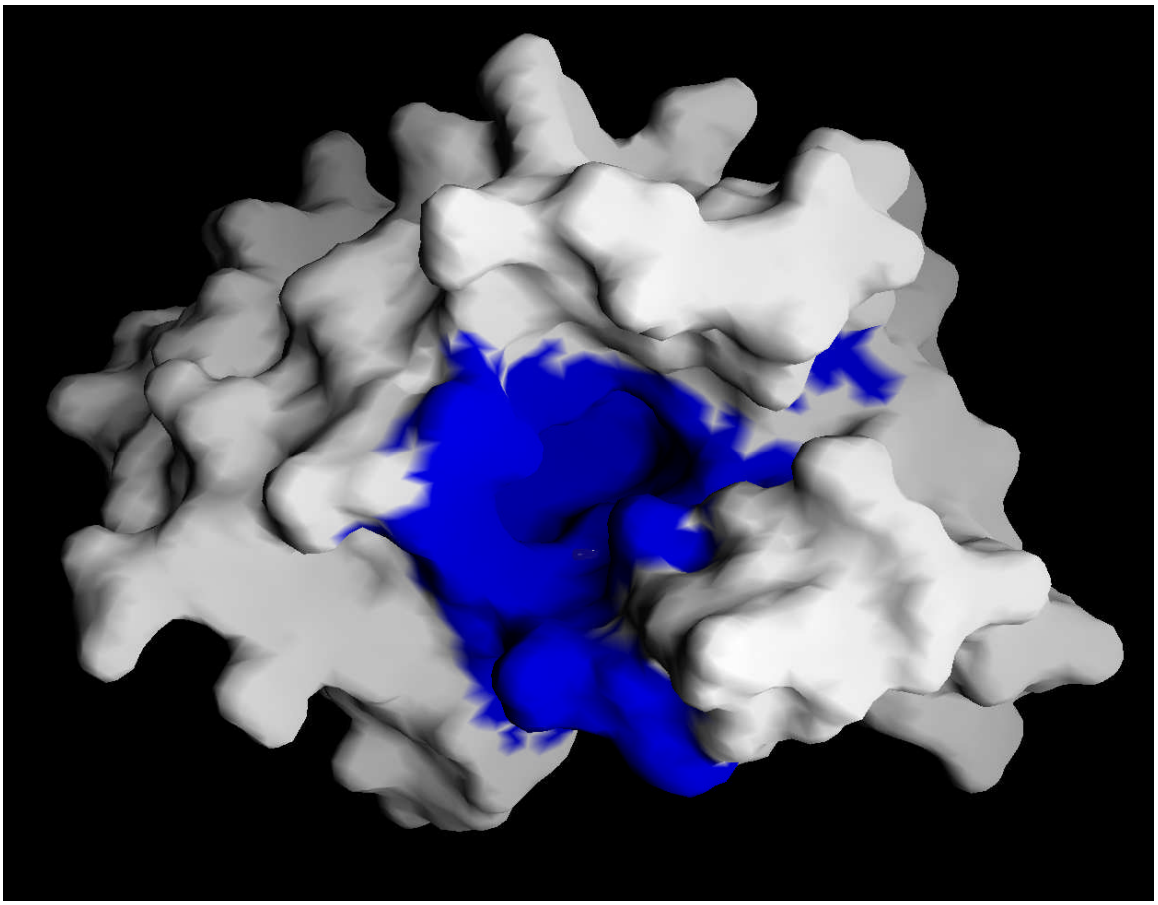

Figure 2.4: Conserved residues of *At*DEF1. The blue represents the conserved residues and the non-conserved residues are in violet, but are not shown because they are on the other side of the enzyme. The blue gives a more specific idea of the enzyme's active site.[42]

2.2.3 Conservation for *E. coli* DEF2

The third mapping involved the conserved residues of *Ecoli*DEF2 (Figure 2.5).[41] Again the blue represents the conserved residues and the violet represents the non-conserved residues.

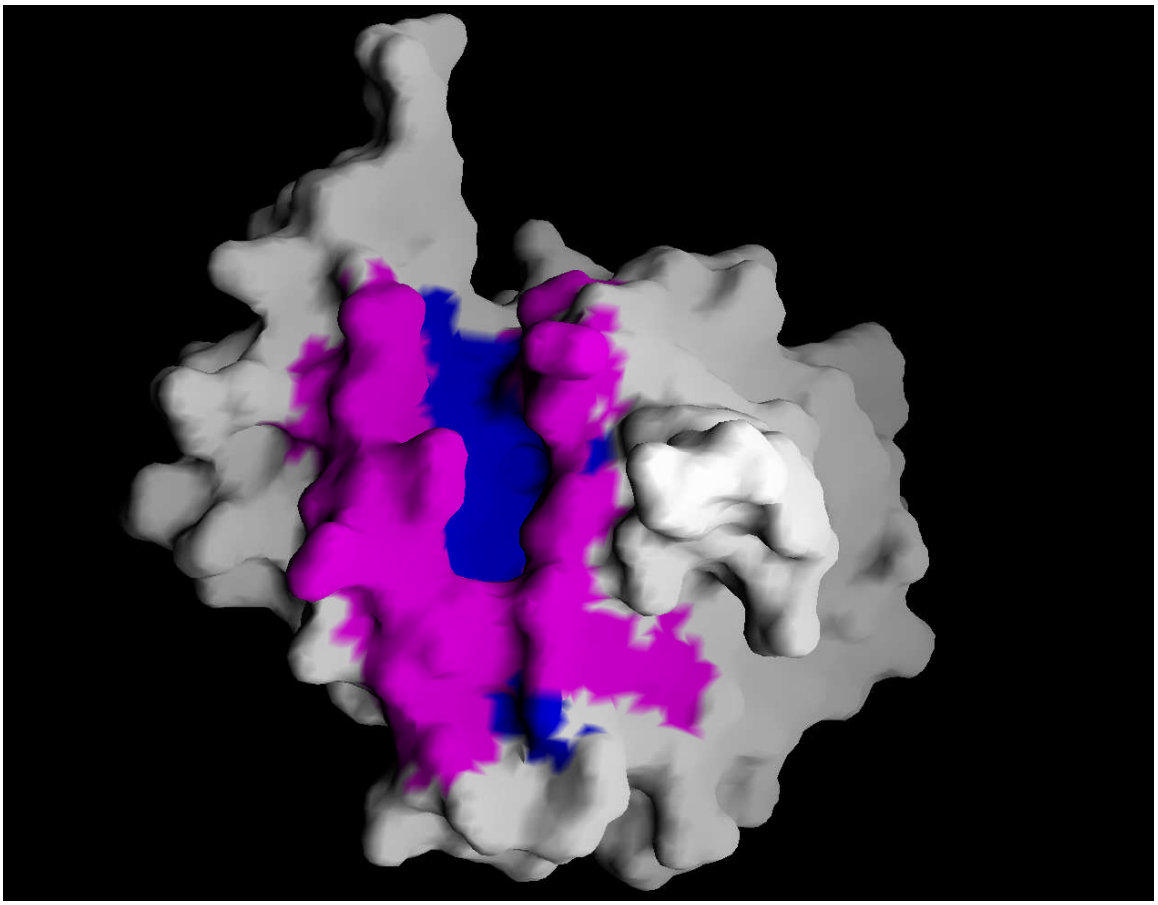

Figure 2.5: Conserved residues of *Ecoli*DEF2. The blue represents the conserved residues and the non-conserved residues are in violet. The blue provides a more specific idea of the enzyme's active site.[41]

2.3 Comparing plantDEF2's Conserved Residues with plantDEF1 and bacteriaDEF2 Residues

Now that we had an idea of what each respective PDF active site looked like, we could then begin to compare and contrast both the plantDEF1 and the bacteriaDEF2 majority and matching residues with those of plantDEF2 that were conserved. This provided more insight into how different plantDEF1 and bacteriaDEF2 were from plantDEF2 and whether or not it would be possible to differentiate between them enough to design an inhibitor that would be selective only to plantDEF2 and not bacteriaDEF2, nor plantDEF1. The main point we were looking for was a difference in specific residues that we could hone in on and take advantage of so we could design an inhibitor specific to plantDEF2 and not to bacteriaDEF2. In the case of plantDEF2 vs. plantDEF1, we

wanted to try and find specific residues that were consistently different between the two enzymes that might explain plantDEF2's preference for the D1 photosystem-II protein as a substrate, while plantDEF1 exhibits no such preference.

2.3.1 Comparison between Plant DEF2 and DEF1

The three motifs of plantDEF2, residues 119-133, 165-178, and 205-219, were compared with the three motifs of plantDEF1, 45-59, 105-118, and 145-159. More specifically, we wanted to see if we could find active site residues that were conserved in plantDEF2 that were not conserved and not the majority residue in plantDEF1 in order to be able to identify residues that could be used to explain why plantDEF2 prefers the D1 substrate and plantDEF1 does not. Table 2.1 shows this comparison where the red X's indicate the low match (20% or less) between plantDEF2's conserved residues and plantDEF1's corresponding residues.

Table 2.1: plantDEF2 vs. plantDEF1. The three motifs of both enzyme's are compared where the red X indicates conserved residues in *At*DEF2 and the corresponding low matching (20% or less) residue in *At*DEF1, whether or not it was conserved

plantDEF2 vs. plantDEF1															
Motif 1: 119-133 (AtDEF2 numbers)															
AtDEF1 residue #	45	46	47	48	49	50	51	52	53	54	55	56	57	58	59
AtDEF2 residue#	119	120	121	122	123	124	125	126	127	128	129	130	131	132	133
Conserved DEF2 Residue (50% or higher)	**T**	**D**	**G**	**I**	**G**	**L**	**S**	**A**	**P**	**Q**	**V**	**G**	**L(n.c.)**	**N**	**V**
Majority Residue in DEF1 Motif	A(31/34)	P(33/34)	G(32/34)	V(27/34)	G(31/31)	L(31/31)	A(31/31)	A(31/31)	P(31/31)	Q(31/31)	I(28/31)	G(31/31)	I(16/32)	P(30/33)	L(30/34)
Number of DEF1 Residues that Matched DEF2	T(0)	D(0)	G(32/34)	I(0)	G(31/31)	L(31/31)	S(0)	A(31/31)	P(31/31)	Q(31/31)	V(0)	G(31/31)	L(1/32)	N(0)	V(0)
Low Match(20% or less) b/w DEF1 and DEF2	X	X		X			X				X		NC	X	X
Motif 2: 165-178 (AtDEF2 numbers)															
AtDEF1 residue#	105	106	107	108	109	110	111	112	113	114	115	116	117	118	
AtDEF2 residue#	165	166	167	168	169	170	171	172	173	174	175	176	177	178	
Conserved DEF2 Residue (50% or higher)	**V(n.c.)**	**P(n.c.)**	**F**	**D(n.c.)**	**E**	**G**	**C**	**L**	**S**	**F**	**P**	**G**	**I**	**Y**	
Majority Residue in DEF1 Motif	A(41/41)	L(21/42)	F(41/42)	F(33/42)	E(42/43)	G(41/43)	C(42/43)	L(41/43)	S(39/41)	V(39/41)	D(31/40)	G(39/40)	F(24/40)	R(36/39)	
Number of DEF1 Residues that Matched DEF2	V(0)	P(0)	F(41/42)	D(0)	E(42/43)	G(41/43)	C(42/43)	L(41/43)	S(39/41)	F(0)	P(2/40)	G(39/40)	I(0)	Y(0)	
Low Match(20% or less) b/w DEF1 and DEF2	NC	NC		NC						X	X		X	X	
Motif 3: 205-219 (AtDEF2 numbers)															
AtDEF1 residue#	145	146	147	148	149	150	151	152	153	154	155	156	157	158	159
AtDEF2 residue#	205	206	207	208	209	210	211	212	213	214	215	216	217	218	219
Conserved DEF2 Residue (50% or higher)	**S(n.c.)**	**L**	**P**	**A**	**R**	**I(n.c.)**	**F**	**Q**	**H**	**E**	**Y(n.c.)**	**D**	**H**	**L**	**E(n.c.)**
Majority Residue in DEF1 Motif	G(33/35)	W(34/35)	Q(29/35)	A(33/34)	R(33/34)	I(33/34)	L(33/33)	Q(32/33)	H(32/33)	E(31/32)	Y(27/31)	D(29/30)	H(29/30)	L(28/29)	E(13/29)
Number of DEF1 Residues that Matched DEF2	S(0)	L(0)	P(0)	A(33/34)	R(33/34)	I(33/34)	F(0)	Q(32/33)	H(32/33)	E(31/32)	Y(27/31)	D(29/30)	H(29/30)	L(28/29)	E(13/29)
Low Match(20% or less) b/w DEF1 and DEF2	NC	X	X				X								
Note: The 'NC' and 'n.c.' in the charts above refer to non-conservation between the AtDEF2 sequence versus the other DEF2 plant sequences.															

One can see there are 14 residues that were conserved in plantDEF2 that hardly showed up in the database screening for plantDEF1 residues. These specific residues are of keen interest because they represent consistent differences between the two enzymes. Figures 2.6 (molecular surface) and 2.7 (ribbons) show a pictorial representation of the low matching residues on the AtDEF2 structure.

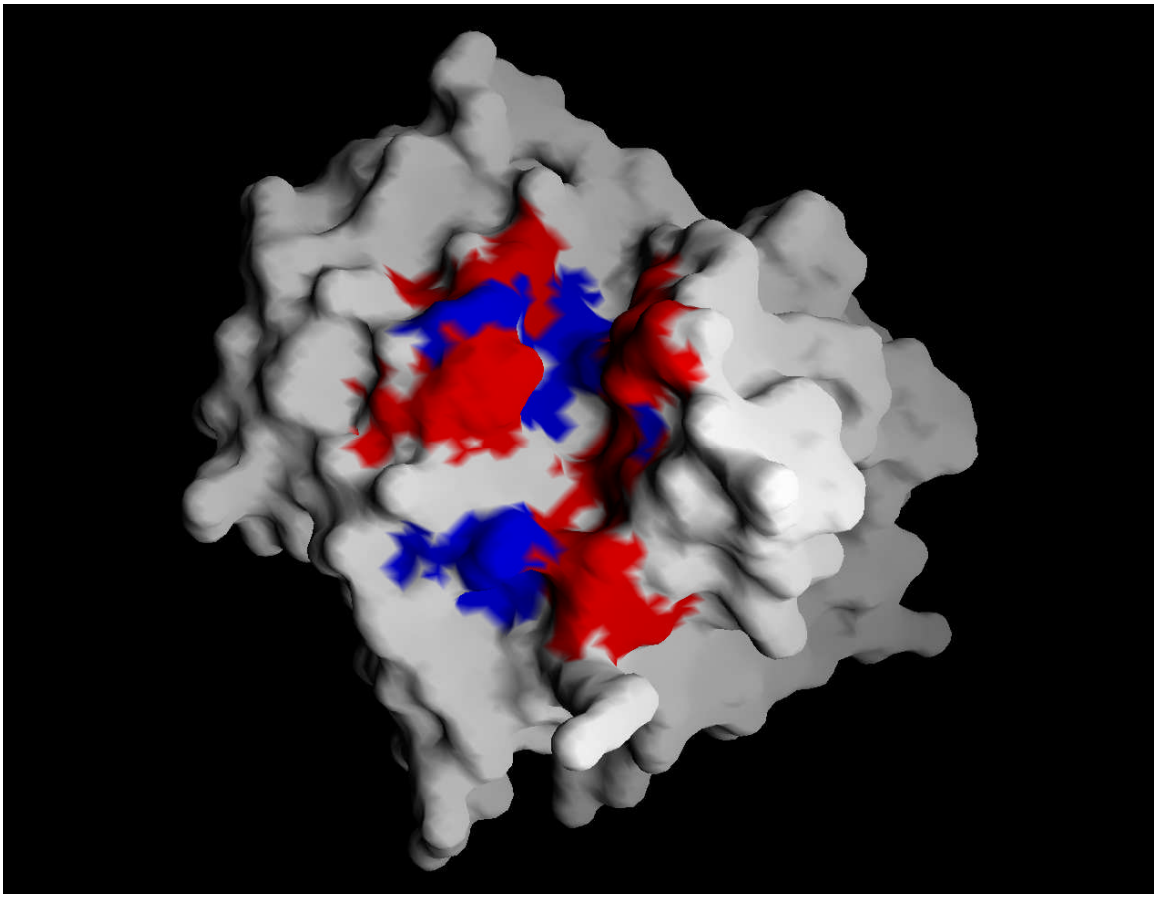

Figure 2.6: Low matching residues on *At*DEF2. The red represents the low matching residues found in plantDEF2 when compared to the residues in plantDEF1. Both red and blue represent the originally conserved residues found in *At*DEF2, which were shown as all blue in Figure 2.2.

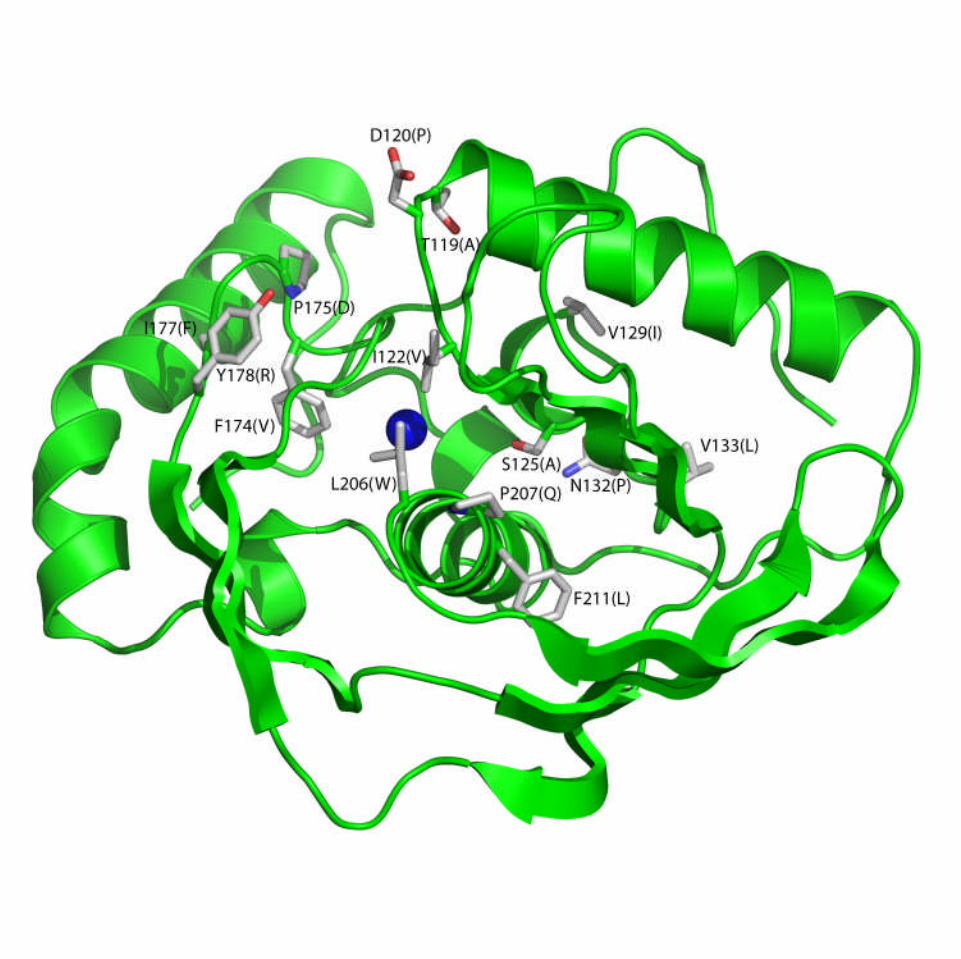

Figure 2.7: Ribbons View of the low matching residue side chains on *At*DEF2. The side chains represent the low matching residues found in plantDEF2 when compared to the residues in plantDEF1. The labels represent the conserved residues in plantDEF2 and the majority residues of plantDEF1 are in parentheses.

2.3.2 Comparison between plantDEF2 and bacteriaDEF2

The three motifs of plantDEF2 were compared with the three motifs of bacteriaDEF2. Again, we wanted to see if we could find residues that were conserved in plantDEF2 that were not conserved and not the majority residue in bacteriaDEF2 in order to be able to identify residues that could be used for inhibitor design. Table 2.2 shows this comparison where the red X's indicate the low match (20% or less) between plantDEF2's conserved residues and bacteriaDEF2's corresponding residues.

Table 2.2: plantDEF2 vs. bacteriaDEF2. The three motifs of both enzyme's are compared where the red X indicates conserved residues in plantDEF2 and the corresponding low matching (20% or less) residue in bacteriaDEF2, whether or not it was conserved.

plantDEF2 vs. bacteriaDEF2															
Motif 1: 119-133 (AtDEF2 numbers)															
EcoliDEF2 residue #	41	42	43	44	45	46	47	48	49	50	51	52	53	54	55
AtDEF2 residue#	119	120	121	122	123	124	125	126	127	128	129	130	131	132	133
Conserved DEF2 Residue (50% or higher)	**T**	**D**	**G**	**I**	**G**	**L**	**S**	**A**	**P**	**Q**	**V**	**G**	**L(n.c.)**	**N**	**V**
Majority Residue in bacteriaDEF2 Motif	A(43/99)	R(26/99)	G(94/100)	V(59/100	G(97/10(	L(85/10(	A(92/10(	A(97/10(	P(57/10(	Q(94/10(	V(45/10(	G(70/10(	V(31/10(	S(27/10(	K(41/100)
Number of bacteria Residues that Matched DEF2	T(2/99)	D(16/99)	G(94/100)	I(33/100)	G(97/10(	L(85/10(	S(1/100)	A(97/10(	P(57/10(	Q(94/10(	V(45/10(	G(70/10(	L(14/10(	N(6/100)	V(6/100)
Low Match(20% or less) b/w Bacteria and DEF2	X	X					X						NC	X	X
Motif 2: 165-178 (AtDEF2 numbers)															
EcoliDEF2 residue #	84	85	86	87	88	89	90	91	92	93	94	95	96	97	
AtDEF2 residue#	165	166	167	168	169	170	171	172	173	174	175	176	177	178	
Conserved DEF2 Residue (50% or higher)	**V(n.c.)**	**P(n.c.)**	**F**	**D(n.c.)**	**E**	**G**	**C**	**L**	**S**	**F**	**P**	**G**	**I**	**Y**	
Majority Residue in bacterialDEF2 Motif	L(21/99)	T(22/99)	G(19/99)	G(23/100	E(100)	G(99/10(	C(92/10(	L(90/10(	S(98/10(	V(47/10(	P(76/10(	G(43/00)	V(32/10(	Y(31/100)	
Number of bacteria Residues that Matched DEF2	V(9/99)	P(5/99)	F(9/99)	D(3/100)	E(100)	G(99/10(	C(92/10(	L(90/10(	S(98/10(	F(9/100)	P(76/10(	G(43/00)	I(11/100)	Y(31/100)	
Low Match(20% or less) b/w Bacteria and DEF2	NC	NC	X	NC						X			X		
Motif 3: 205-219 (AtDEF2 numbers)															
EcoliDEF2 residue#	124	125	126	127	128	129	130	131	132	133	134	135	136	137	138
AtDEF2 residue#	205	206	207	208	209	210	211	212	213	214	215	216	217	218	219
Conserved DEF2 Residue (50% or higher)	**S(n.c.)**	**L**	**P**	**A**	**R**	**I(n.c.)**	**F**	**Q**	**H**	**E**	**Y(n.c.)**	**D**	**H**	**L**	**E(n.c.)**
Majority Residue in Bacteria Motif	G(75/100)	L(36/100)	L(44/100)	A(90/100	R(46/10(	V(37/10(	I(43/100)	Q(90/10(	H(100)	E(97/10(	I(46/100)	D(95/10(	H(92/10(	L(86/10(	N(48/100)
Number of bacteria Residues that Matched DEF2	S(3/100)	L(36/100)	P(15/100)	A(90/100	R(46/10(	I(11/100)	F(14/10(	Q(90/10(	H(100)	E(97/10(	Y(7/100)	D(95/10(	H(92/10(	L(86/10(	E(7/100)
Low Match(20% or less) b/w Bacteria and DEF2	NC		X			NC	X				NC				NC
Note: The 'NC' and 'n.c.' in the charts above refer to non-conservation between the AtDEF2 sequence versus the other DEF2 plant sequences.															

One can see there are 10 residues that were conserved in plantDEF2 that hardly showed up in the database screening for plantDEF1 residues. These specific residues are of keen interest because they represent consistent differences between the two enzymes. Figures 2.8 (molecular surface) and 2.9 (ribbons) show a pictorial representation of the low matching residues on the AtDEF2 structure.

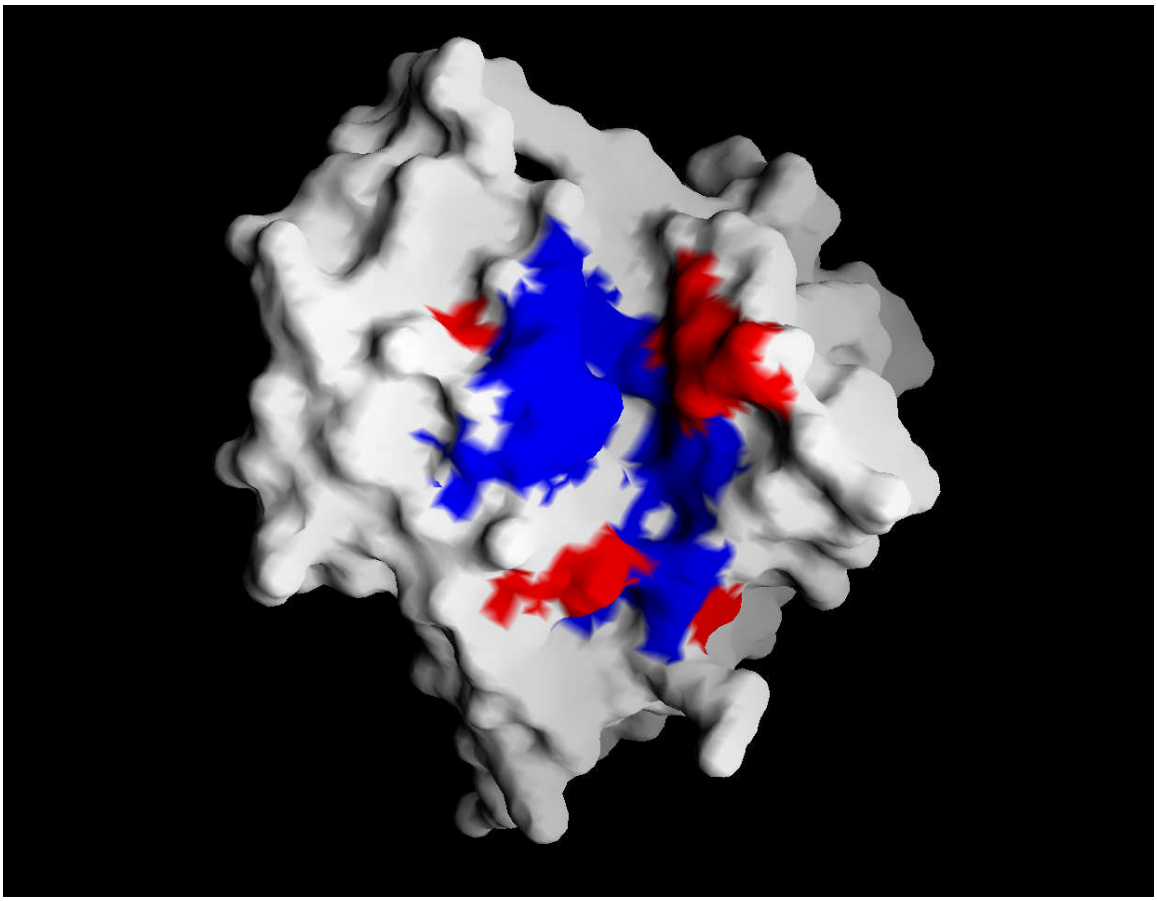

Figure 2.8: Low matching residues on *At*DEF2. The red represents the low matching residues found in plantDEF2 when compared to the residues in bacteriaDEF2. Both red and blue represent the originally conserved residues found in *At*DEF2, which were shown as all blue in Figure 2.2.

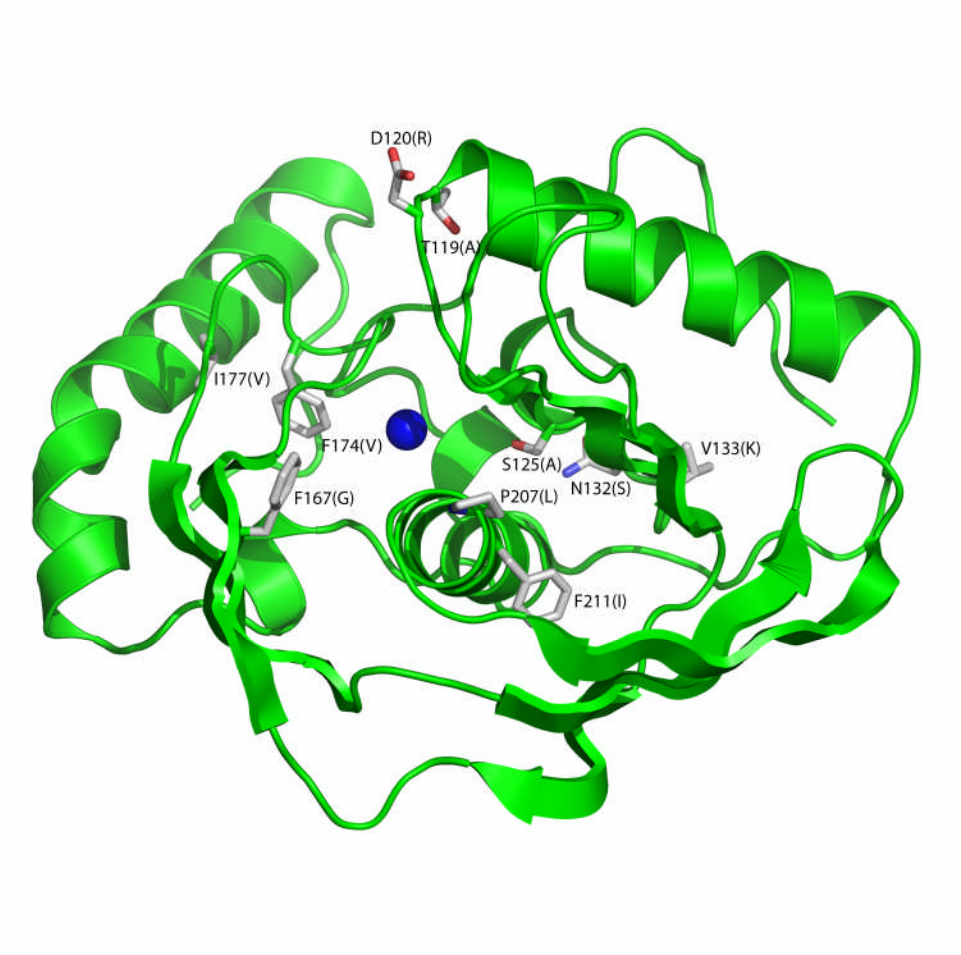

Figure 2.9: Ribbons View of the low matching residues' side chains on *At*DEF2. The side chains represent the low matching residues found in plantDEF2 when compared to the residues in bacteriaDEF2. The labels represent the conserved residues in plantDEF2 and the majority residues of bacteriaDEF2 are in parentheses.

2.4 plantDEF2 Non-Conserved Residues Investigation

In order to make sure there were no residues in the three motifs of plantDEF2 that were not being taken full advantage of, a non-conserved analysis was performed. This involved checking what the next two highest residues were in plantDEF2 for that particular position against the two majority residues for bacteriaDEF2. If a residue showed up in many plantDEF2 sequences, but was not conserved, it still might be useful as long as it also didn't show up in many bacteriaDEF2 sequences (Table 2.3).

Table 2.3: Investigation into the Non-Conserved Residues of plantDEF2 as Compared to bacteriaDEF2. At the top of the chart are portions of the three motifs of plantDEF2. There it can be seen which residues are the non-conserved (n.c.) ones. At the bottom of the chart are the bacteriaDEF2 1st and 2nd majority residues as well as the residues that are found in bacteriaDEF2 that matched the conserved plantDEF2 residues. From this diagram it can be inferred that the residues that come up most often in place of the non-conserved residues of plantDEF2 are also virtually the same as the majority residues found in bacteriaDEF2.

	Low Matching Residues From plantDEF2																	
	Motif 1: 119-133						Motif 2:165-178						Motif 3: 205-219					
RES	119	120	125	131 (n.c.)	132	133	165 (n.c.)	166 (n.c.)	167	168 (n.c.)	174	177	205 (n.c.)	207	210 (n.c.)	211	215 (n.c.)	219 (n.c.)
	42	42	43	44	44	44	43	43	42	43	42	40	36	36	36	36	35	32
#	T	D	S	L	N	V	V	P	F	D	F	I	S	P	I	F	Y	E
A	1	1	1										3					
C																		
D	1	41						1		4			7					
E							4			18			4					6
F									28		42			1		36	26	
G									1				15					
H														1				
I				17			6	2				39			14			
K													1					
L				3			6	13				1						3
M				8														
N					43					17				2				
P								15						24				
Q														1				21
R							4						5					2
S			42		1		3			1			1	6	1			
T	40						7			3								
V				16		44	13	12						1	21			
W																		
Y									13								9	
Bacteria	**41**	**42**	**47**	**53**	**54**	**55**	**84**	**85**	**86**	**87**	**93**	**96**	**124**	**126**	**129**	**130**	**134**	**138**
Maj1	A(43/99)	R(26/99)	A(92/100)	V(31/100)	S(27/100)	K(41/100)	L(21/99)	T(22/99)	G(19/99)	G(23/100)	V(47/100)	V(32/100)	G(75/100)	L(44/100)	V(37/100)	I(43/100)	I(46/100)	N(48/100)
Maj2	L(18/99)	P(20/99)	T(4/100)	I(30/100)	P(21/100)	L(29/100)	I,Q(11/99)	S(18/99)	Y(17/99)	E(22/100)	I(30/100)	Y(16/100)	D(11/100)	P(15/100)	C(33/100)	V(20/100)	M(15/100)	D(22/100)
Def2	T(2/99)	D(16/99)	S(1/100)	L(14/100)	N(6/100)	V(6/100)	V(9/99)	P(5/99)	F(9/99)	D(3/100)	F(9/100)	I(11/100)	S(3/100)	P(15/100)	I(11/100)	F(14/100)	Y(7/100)	E(7/100)

This analysis shows that the residues that come up most often in place of the non-conserved residues of plantDEF2 are also virtually the same as the majority residues found in bacteriaDEF2. This means they can *not* be taken advantage of to try and further find differences between the two for inhibitor selectivity purposes.

2.5 Modeling the Preferred D1 Substrate into an *At*DEF2 Model

To get an idea of the possible interactions the preferred D1 substrate might encounter in the *At*DEF2 enzyme, we modeled in a generic MTAIL sequence molecule based on a formyl-Met-Ala-Ser ligand alignment found in the protein data base (figure 2.10).[46] It is important to note that bacterial enzyme conformations did not change much whether a ligand was bound or not. This logic was applied to this study where an

unbounded AtDEF2 enzyme was overlapped with a bacteriaDEF2 enzyme that already had a tripeptide bound in order to get a general idea of MTAIL interactions. Doing this would allow us an idea, at least near the active site, of any low matching residues of plantDEF2 that might interact directly with the D1 substrate.

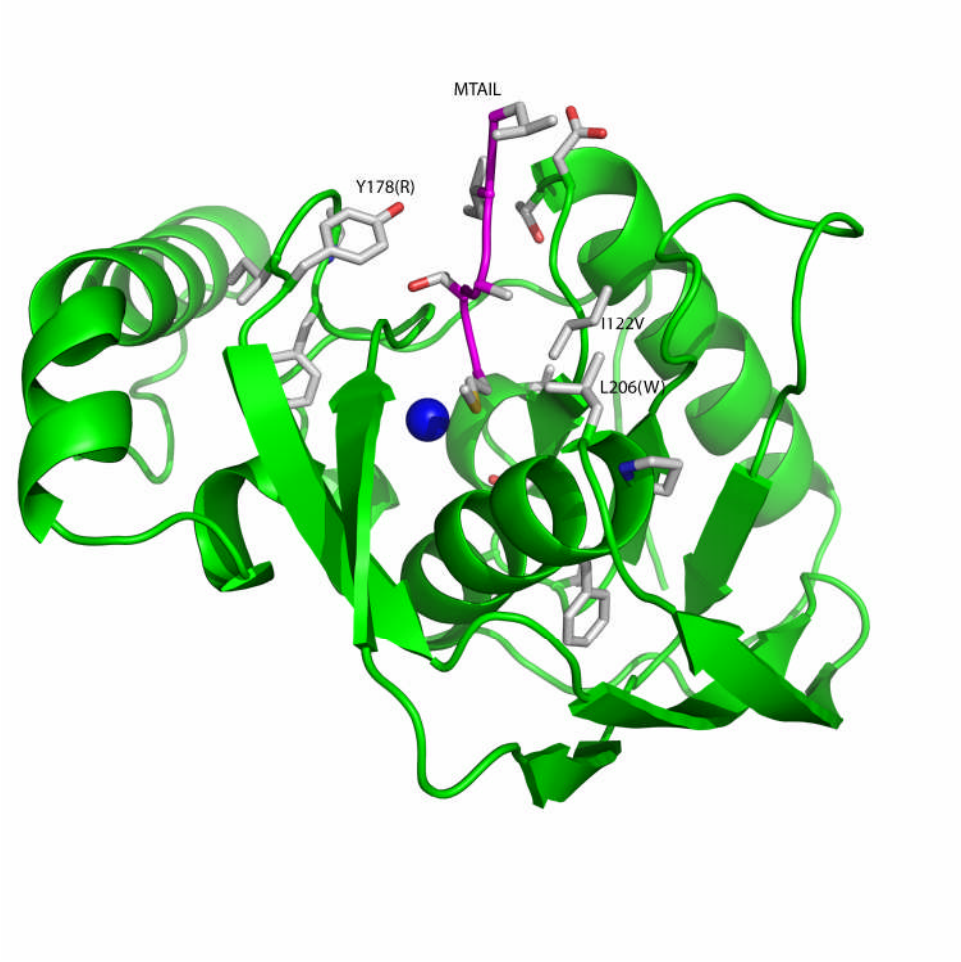

Figure 2.10: A ribbons view of *At*DEF2 with a generic MTAIL (D1) peptide inserted. From this generic diagram it can be hypothesized that the tyrosine residue at 178 might have an H-bonding interaction with the threonine hydroxyl group of the D1 substrate. This might be something that can be taken advantage of when trying to design an *At*DEF2 specific inhibitor.

From this generic diagram, it can be hypothesized that the tyrosine residue at 178 might have an H-bonding interaction with the threonine hydroxyl group of the D1 substrate. This interaction might be one of the reasons why plantDEF2 prefers the D1 substrate. In order to understand the low matching residue interactions with the D1

substrate better, a molecular dynamics experiment would need to be performed. This would allow one an idea of what the energy minimized binding of the D1 substrate might look and act like and tell us more specifically of any particular residues that influence this process more than others. Current research being done at the time of writing involves the running of molecular dynamics experiments with all of the enzyme's atoms fixed and with them moving freely. Other research being performed at the time of writing was a mutagenesis experiment. This experiment replaces that specific residue in plantDEF2 and it might be possible to determine the direct relevance of that particular residue.

Chapter 3: Design, Synthesis, and Purification of PDF Inhibitors

3.1 Synthesis of a Known Thiol Inhibitor

When I first started this project, I was asked if I could synthesize one of Pei's inhibitors **29b** (Scheme 3.1), which was mentioned in the introductory chapter.[32] The purpose of this exercise was to be able to test a novel thiol inhibitor against plant PDF to see how effective it would be. More specifically, to see if Pei's most potent thiol inhibitor would be more effective than actinonin (**1**) during in vivo leaf painting studies. The following represents that synthesis (scheme 3.1).

The synthesis of the chelating portion of the thiol inhibitor[32] started with a fairly trivial butylation of dimethyl malonate **21** (69%) followed by hydrolysis to form malonic acid **23**. From there, paraformaldehyde and dimethylamine were used along with refluxing to induce decarboxylation and form the α,ß-unsaturated acid **24** (63% over two steps). For the final step in creating the chelating portion, thiolacetic acid was added to the acid **24** to give the acetyl-protected thiol acid **25** via conjugate addition.

The synthesis of the remaining backbone portion involved the coupling of *p*-nitroaniline with the *N*-Fmoc(fluorenylmethyloxycarbonyl)-protected acid **26b** using phosphorus oxychloride, imidazole, and pyridine. This product was then deprotected with a 20% piperidine/dichloromethane solution to yield the coupled amine **27b** (60% yield over two steps).

Next, the two portions were coupled using dicyclohexylcarbodiimide (DCC) to give the protected thiol **28b** (92%). Next, the protected thiol **28b** was reduced using sodium borohydride in ethanol. This product was quenched with water and 5% HCl and worked up and carried over to the next reaction with no chromatography. Finally, the *N*-Boc group was removed using trifluoracetic acid (TFA) in dichloromethane to give the final desired product **29b** (74% over two steps).

Scheme 3.1: Synthesis of a Potent Thiol Inhibitor 29b.[32]

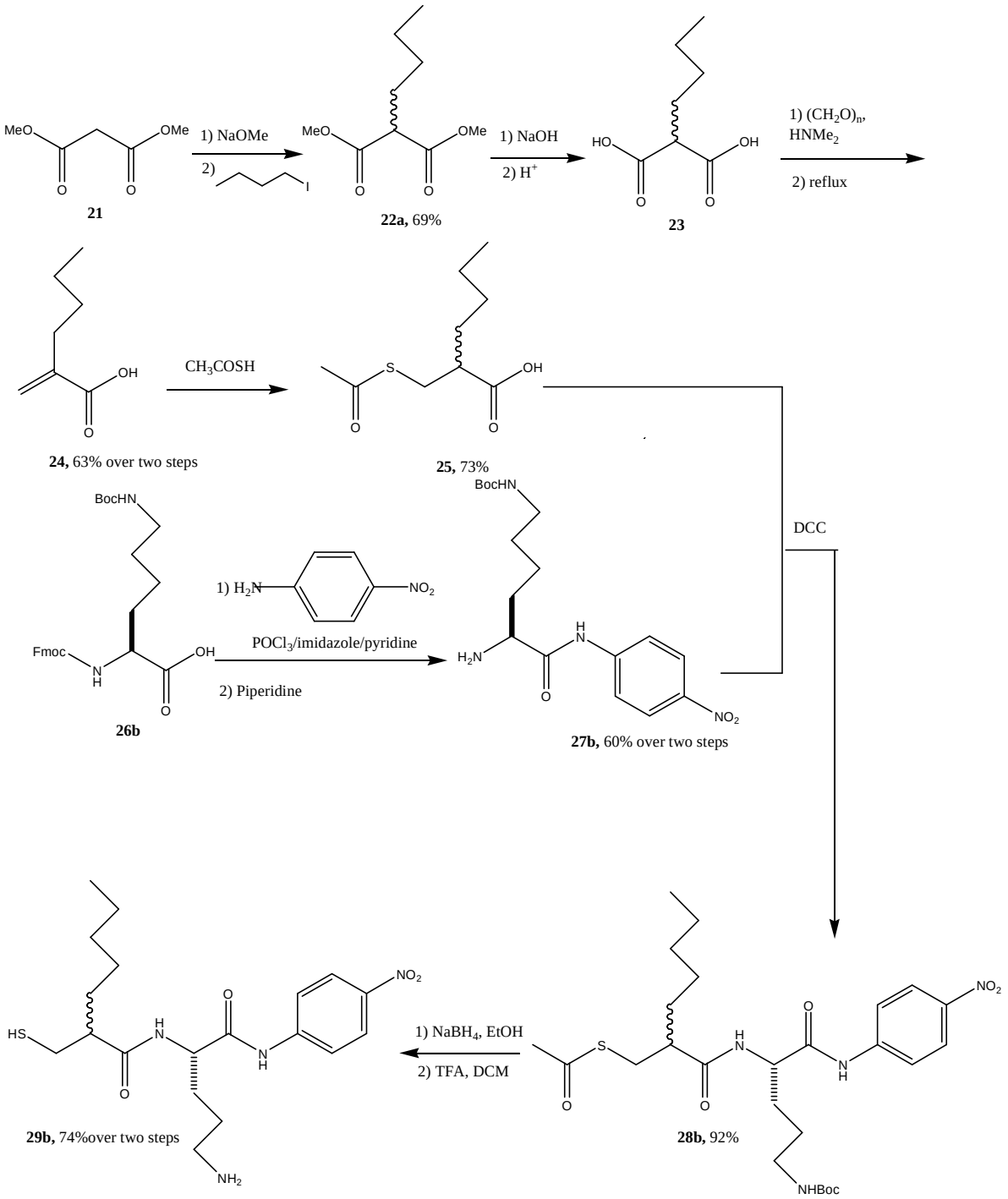

3.2 Design, Synthesis, and Purification of a Novel Thiol-Actinonin Chimera 34

The design and synthesis of the peptide-based inhibitors were conceived and performed in concert with the computational active site analysis. This synthesis was followed with purification and biological analysis to determine the potency of the inhibitor, which is discussed later in chapter 4.

3.2.1 Design of a Novel Thiol-Actinonin Chimera 34

Due to the efficacy of actinonin **1** during in vitro studies (*E. coli* Ni-PDF: IC_{50} = 3 nM, MIC = 25 nM, K_I = 0.28 nM)[20] (*At*DEF2 Ni-PDF: IC_{50} = 50-100 nM, MIC = 25 nM)[23] and its inefficiency during in vivo studies[26], it was proposed that the hydroxamate chelating group responsible for metabolism of the inhibitor be removed altogether. Through the accomplishments of Pei et al. [32] it was believed that thiol inhibitors could survive in vivo and also prove to be fairly potent. Therefore, the design for our first novel inhibitor was envisaged to possess the peptide backbone of actinonin and the chelating thiol group from Pei's most potent inhibitor **29b (***E. coli* Ni-PDF: MIC = 75-100 μM, K_I = 19 nM)[32] (Figure 3.1).

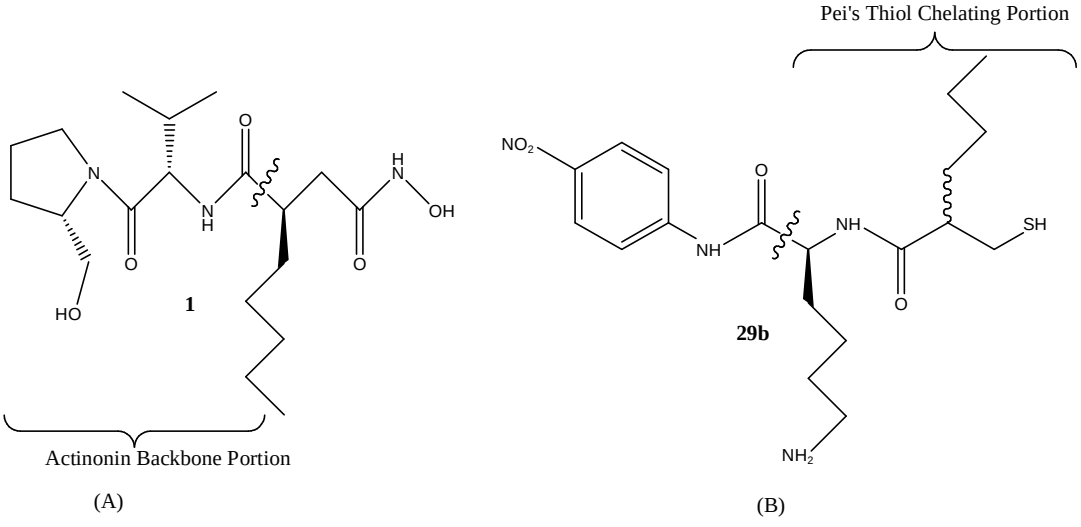

Figure 3.1: Structural Comparison between Actinonin (A) 1 and Pei's Thiol Inhibitor (B) 29b.

This combination of the two portions might allow for a tight binding to the *At*DEF2 active site due to the side chains of actinonin and the chelating group found in Pei's thiol inhibitors. The result would be a novel actinonin chimera **34** (figure 3.2).

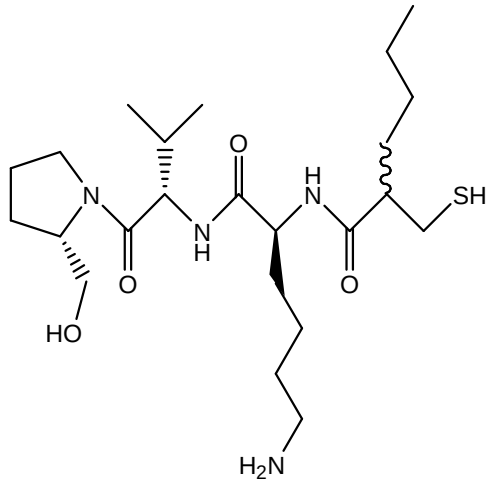

Figure 3.2: Thiol-Actinonin Chimera 34.

3.2.2 Synthesis of a Novel Thiol-Actinonin Chimera 34

The synthesis of **34** begins with L-prolinol (**7**) (scheme 3.2). *L*-prolinol (**7**) was coupled with N-benzyloxycarbonyl-L-valine *p*-nitrophenylester (**8**) at room temperature to give the *N*-CBZ (benzyloxycarbonyl)-protected amine **9** in nearly quantitative yields.[15] Anderson's route for the next step involves a reduction using 10% palladium-charcoal and thermal decarboxylation, which forms a carbamic acid intermediate, whereas I preferred the easier route using 10% Pd/C and a high pressure bomb hydrogenator with ~350-500 psi H_2 to deprotect the *N*-CBZ group to form the primary amine **2** (96%).

Scheme 3.2: Synthesis of L-Valyl-L-Prolinol (2) Used to Make the Actinonin Chimera 34.

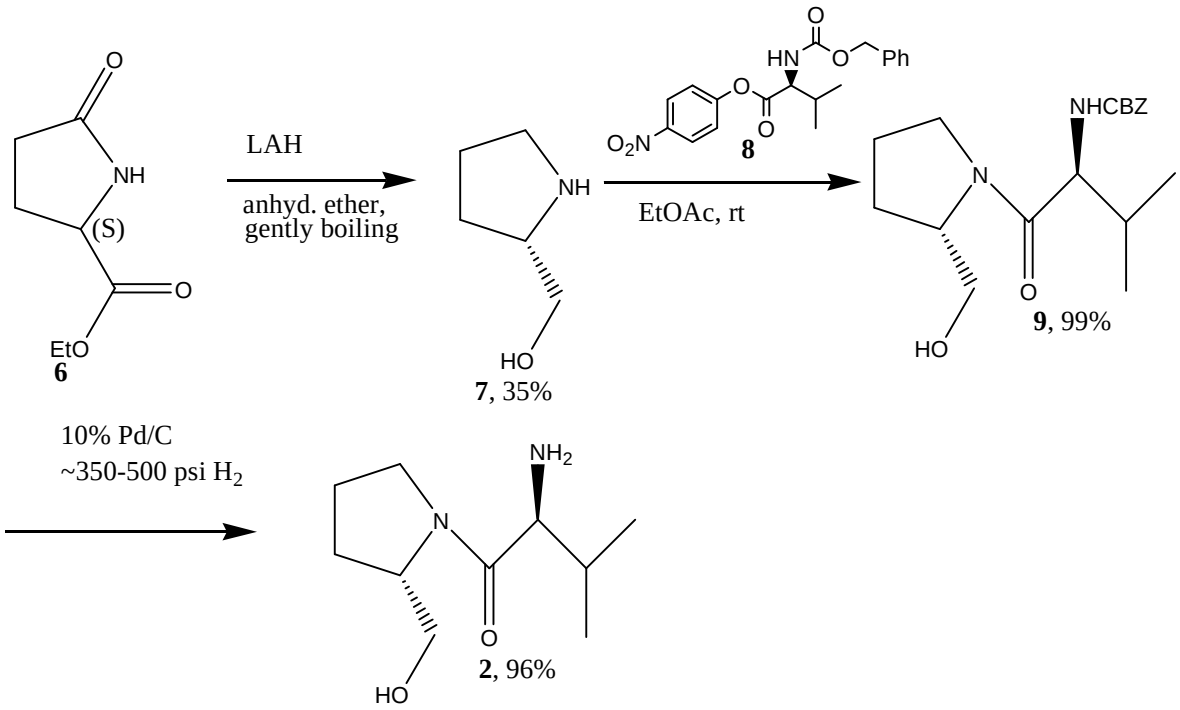

Once the primary amine **2** had been synthesized, it was coupled to *N*-Fmoc-L-Lys(Boc)-OH (**30**) using DCC in dichloromethane, instead of using Pei's route of using $POCl_3$/imidazole in pyridine seen in schemes 1.7, 3.1. This reaction step formed the *N*-Fmoc/Boc-protected chimera backbone product **31** (Scheme 3.3). Compound **31** was then deprotected with DMAP in DMF to give the primary amine **32**. Pei's synthesis[32] accomplished a similar deprotection by using a 20% piperidine solution in dichlormethane. However, this did not produce adequate yields for this particular reaction and was therefore changed to a 10% solution of DMAP, which produced the primary amine **32** with little to no starting material observed on the thin layer chromatography (TLC) plates. Product **32** was carried over with excess DMAP into the next reaction, which involved a coupling between compound **32** and the acetyl-protected thiol acid **25** using DCC in dichloromethane once again. This reaction yielded the final coupling product **33** (50% over two steps) (Scheme 3.3).

Scheme 3.3: Synthesis of Acetyl-Protected Thiol Inhibitor 33.

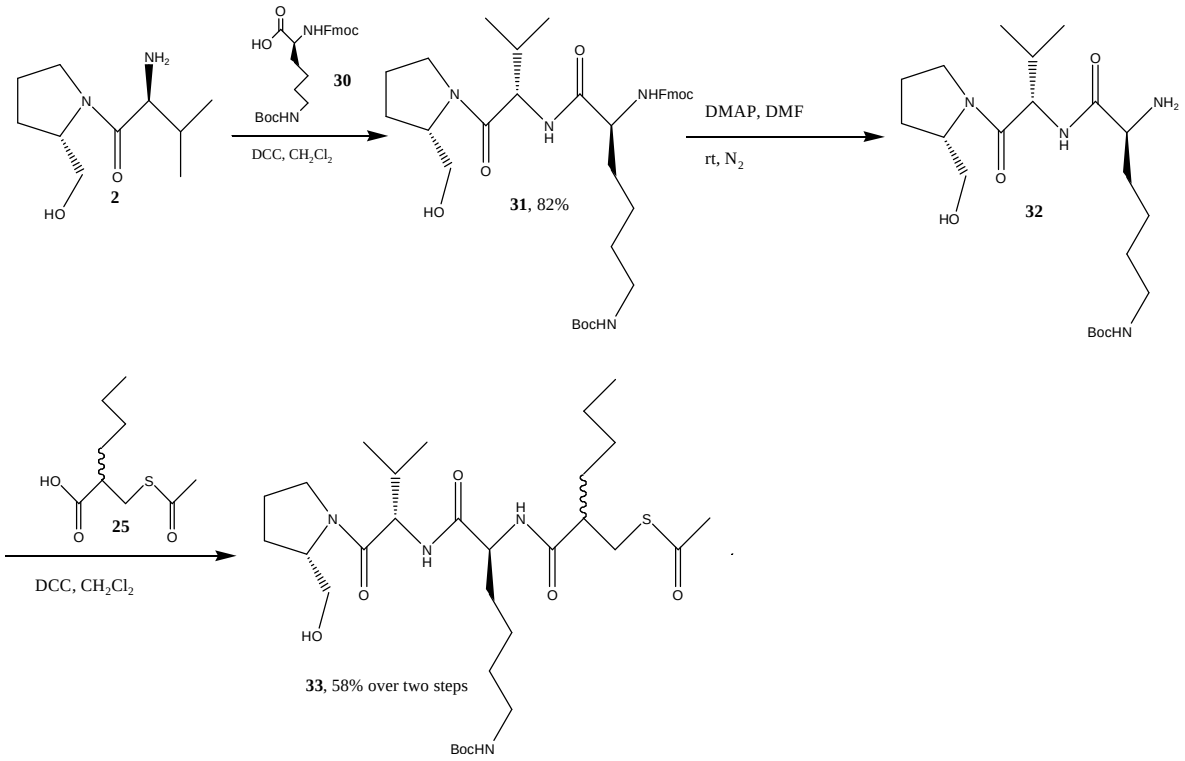

The final two reactions performed on compound **33** involved a reduction of the *S*-acetyl group to form the sulfhydryl group and the removal of the Boc group, leaving the primary amine **34** as the result (scheme 3.4). The reduction was a straightforward reaction using sodium borohydride ($NaBH_4$) in EtOH, while the trifluoracetic acid (TFA) in CH_2Cl_2 was also a fairly trivial reaction that removes the *N*-Boc group.

Scheme 3.4: Synthesis of the Thiol-Actinonin Chimera 34.

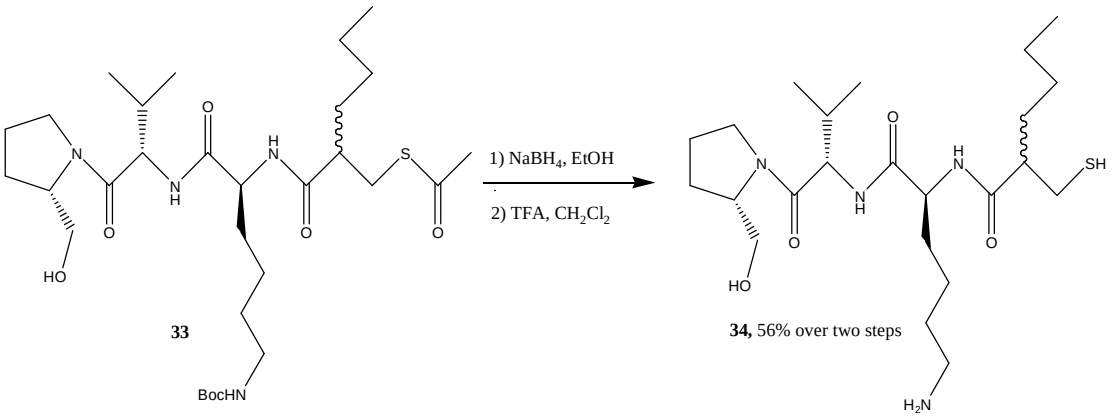

3.2.3 Characterization and Purification of a Novel Thiol-Actinonin Chimera 34

Characterization and purification of the thiol-actinonin chimera **34** was difficult mainly for two reasons. Firstly, several deprotection steps along the way removed much mass causing one to have to push through several grams of material in order to have a decent amount of material at the end of the synthesis. Secondly, due to the polar nature and the slow rotation about to the L-prolinol amide bond, the compounds throughout the synthesis were hard to isolate and characterize. The second reason is the subject of this subsection.

The rotation about the bond between the nitrogen of the L-prolinol group and the adjacent carbon atom of the carbonyl functional group greatly affected the ^{1}H and ^{13}C NMR spectra. Rotation causes less intense peaks to appear very closely in chemical shift to the expected peaks for each product. This occurs because the rotation about the N-C bond is a slow interconversion between rotamers that are approximately equal in energy, but have slightly differing chemical shifts. The effect on the proton spectra was the formation of many multiplets, while the carbon spectra (figures 3.3 and 3.4) showed peaks that were smaller in height and adjacent to the predominant signal peaks. This effect, in combination with the number of protons and carbons associated with each compound throughout the synthesis, caused a great deal of complexity in the NMR analysis. In order to try and alleviate this problem, the NMR solvent used was switched from the usual $CDCl_3$ and d-acetone to d_6-dimethylsulfoxide (d_6-DMSO) and the NMR spectra were taken at 50 °C in order to increase the rate of rotation so that the signals

averaged out and gave one main signal. In order to obtain better proton spectra, the NMR tube could be heated to 100 °C, which would give a finer, more resolved peak instead of a broad multiplet. This increase in temperature to 100 °C has yet to be performed at the time of writing. The mass spectrometry (MS) and reverse-phase high pressure liquid chromatography (RP-HPLC) data also helped support the otherwise qualitative NMR analysis.

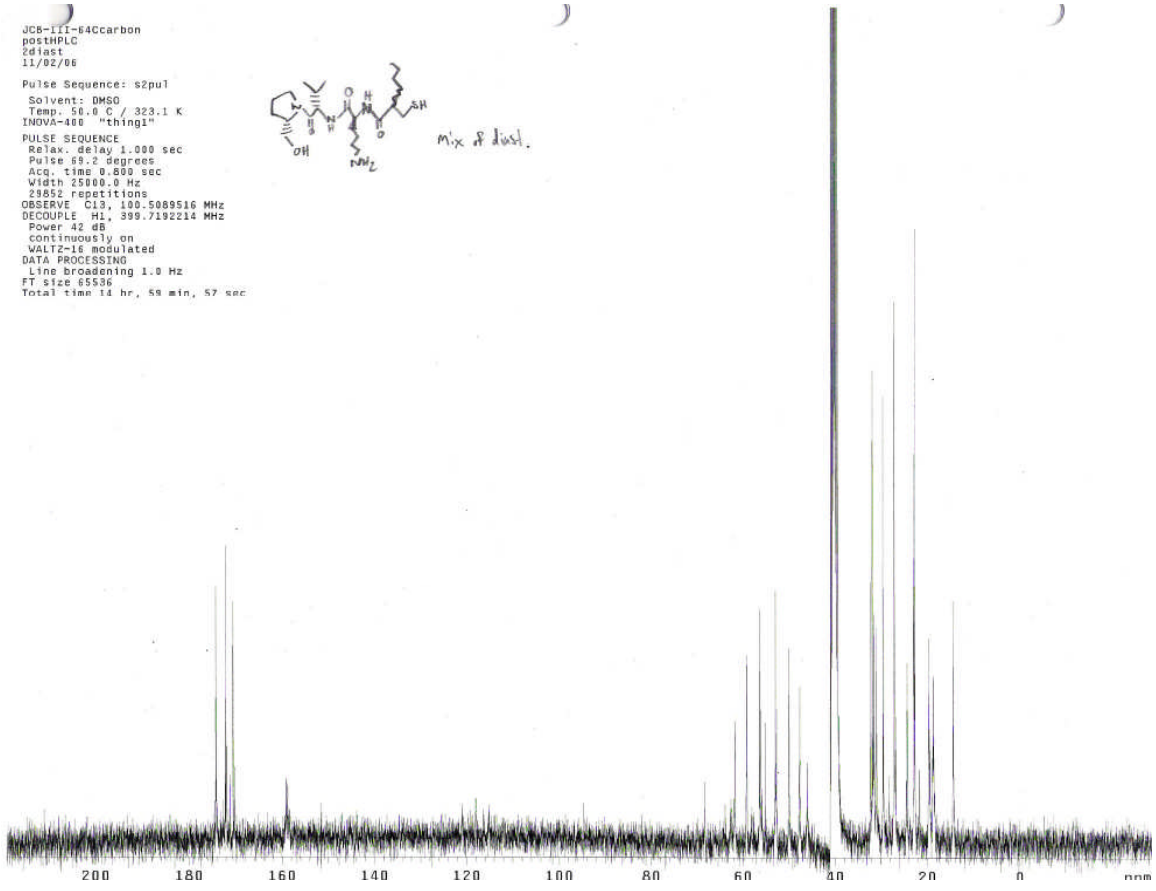

Figure 3.3: Full, Intensified ^{13}CNMR of 34. Note the three amido-carbonyl peaks in the 170 ppm range.

Figure 3.4: Closer view of the three amido-carbonyl peaks of 34 ^{13}CNMR. Note the two-thirds less intense peaks to the right of each labeled peak. The chemical shift labels are in ppm.

The purification of most of the compounds along the line of the synthesis was done mostly via flash chromatography, and the last compound, **34**, was purified via RP-HPLC. The biggest problem encountered when using flash chromatography was that the retention factors (R_f) of the desired products were often very close to the byproducts' R_f values. There were three ways to solve this problem. Firstly, one could reduce the amount of material per reaction in order to run smaller columns, which would allow better resolution between product bands that would be emitted. The problem with this idea, as mentioned earlier, is that one had to use many grams of material to obtain relatively little amounts of product. Secondly, one could run fairly large columns with a very "slow" solvent system (low polarity solvent system), which can be time consuming. Thirdly, after characterization of products along the way, one could skip some chromatographic sessions and simply carry the material on to the next step, so long as the

product spot was interpretable via TLC. The latter two methodologies were employed during the course of the synthesis of the compounds leading up to **34**.

The purification of **34** to obtain the product diastereomers **34a** and **34b** was performed using a reverse-phase C-18 HPLC column with a standard gradient of acetonitrile (0-100%) in 0.1% aq. TFA. The absorbance was monitored at 214 nm. At first, the diastereomers were separated into diastereomer 1 and diastereomer 2 + byproduct (third major peak), but after performing the enzyme assays, which are discussed in chapter 4, it was determined that there was no need to isolate the individual diastereomers because there was not a great difference in potency observed. Therefore the two major peaks of the reaction were collected together with approximately 80-85% purity and characterized via ^{1}H and ^{13}C NMR as well as with +EI-MS and determined to be the two diastereomers of the desired product **34**.

3.3 Experimental Section

HPLC Solutions and Instrumentation

The purification of **34** was performed using a reverse-phase C-18 HPLC column (Prep Scale: VYDAC, Protein and Peptide C18; Analytical Scale: Aquapore, Butyl 7 micron, 220 x 4.6 mm) with a standard 50-minute gradient of acetonitrile (0-100%) in 0.1% aq. TFA at10ml min^{-1}. The absorbance was monitored at 214 nm and the diastereomers collected. The other instruments used in conjunction with the column were a Waters 510 HPLC pump, Waters U6K Millipore, and a Waters Tunable Abs. Detector.

Synthesis/Characterization Procedures/Results

For all of the compounds reported, the 400 MHz ^{1}H NMR and 100 MHz ^{13}C NMR data were collected on a Varian VXR-400S. For all pH values reported, a Denver Instrument pH Meter was used.

The Mass Spectrometry data was obtained by Dr. Jack Goodman of the University of Kentucky Mass Spectrometry Facility. Electron impact (EI) ionization mass spectra were recorded at 70eV on ThermoFinnigan PolarisQ (ion trap mass spectrometer). Samples were introduced via heatable direct probe inlet. Electrospray ionization (ESI) mass spectra were obtained on a ThermoFinnigan LTQ.

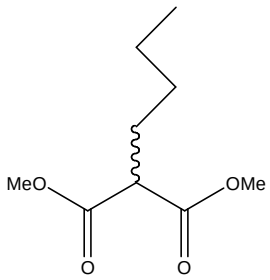

Dimethyl 2-butylmalonate (22a).[32] $C_9H_{16}O_4$. Na metal (2.02 g, 88.0 mmol) was added to dry MeOH (~100 mL) under N_2 at 0 °C. Next, dimethyl malonate (5.02 mL, 44.0 mmol) was added to the reaction mix and stirred for ~ 30 minutes while warming to room temperature. Then, 1-iodobutane (3.41 mL, 30.0 mmol) was added to the reaction mix via cannula from a separate reaction flask also under N_2 and containing MeOH (~50 mL). The reaction was allowed to reflux for 30 minutes, and then the solvent was evaporated and the residue worked up using $^{+}NH_4\,^{-}Cl$ and ether. The organic portion was dried with $MgSO_4$ and filtered. Flash chromatography (10% ethyl acetate in petroleum ether) gave pure **22a** (69% yield). ^{1}H NMR (400 MHz, $CDCl_3$) δ: 3.74 (s, 6H), 3.36 (t, 7.51 Hz, 1H), 1.88-1.94 (m, 2H), 1.24-1.39 (m, 4H), 0.90 (t, 7.05 Hz, 3H). ^{13}C NMR (100 MHz, $CDCl_3$) δ: 169.9, 52.4, 52.3, 29.4, 28.0, 23.7, 13.9.

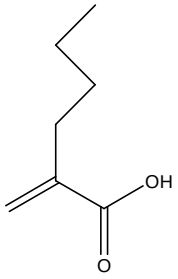

2-(n-Butyl)-acrylic acid (24).[32] $C_7H_{12}O_2$. Dimethyl 2-butylmalonate (**22a**) (1.0 g, 5.3 mmol) was dissolved in a H_2O/MeOH (15 mL of each) solution and NaOH (466 mg, 11.66 mmol) was added and the solution refluxed for ~ 1hr. The flask was cooled to room temperature and the reaction mixture diluted with H_2O (30 mL) and extracted with ethyl acetate (30 mL). The aqueous layer was cooled to 0°C and made to have a pH of 1 via the addition of conc. HCl. The solution was then extracted with ethyl acetate (3 x 20 mL portions) and the combined organic layers were dried via $MgSO_4$, and the solvent

evaporated. The white solid formed **23** was carried over to the next step without flash chromatography, nor NMR analysis. The white solid **23** was dissolved in EtOAc (20 mL), cooled to 0°C. Next, dimethyl amine (752 µl, 15.0 mmol) and paraformaldehyde (300 mg, 10.0 mmol) were added to the reaction mixture and allowed to stir at room temperature for 10 minutes. Then, the reaction was refluxed for 2 hrs. Next, the reaction was cooled to room temperature and quenched with H_2O (30 mL). The solution was cooled to 0°C and conc. HCl was added to make the pH equal to 1. After extraction with ethyl acetate (3 x 30 mL portions), the organic layer was dried with $MgSO_4$ and the solvent evaporated to obtain pure **24** (63% yield over two steps). ^{1}H NMR (200 MHz, $CDCl_3$) δ: 6.24 (s, 1H), 5.62 (s, 1H), 2.30 (t, 7.6 Hz, 2H), 1.23-1.57 (m, 4H), 0.92 (t, 7.0 Hz, 3H). ^{13}C NMR (100 MHz, CDCl3) δ: 173.2, 140.4, 127.4, 31.3, 30.7, 22.5, 14.1.

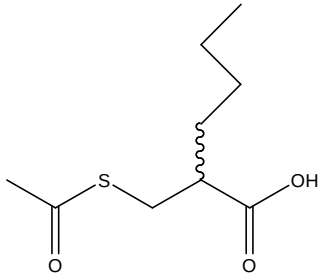

3-Acetylmercapto-2-butylpropionic acid (25).[32] $C_9H_{16}O_3S$. 2-(n-Butyl)-acrylic acid (**24**) (396 mg, 3.09 mmol) was added to thiolacetic acid (330 µl, 4.64 mmol) and refluxed for 2 hrs. Then, the excess thiolacetic acid was evaporated and the residue was dissolved in $NaHCO_3$ (20 mL) and extracted with ethyl acetate (2 x 40 mL portions). Next, the aqueous layer was cooled to 0°C and acidified with HCl to pH 2.18 and extracted with ethyl acetate (2 x 40 mL portions). The organic layer was dried with MgSO4 and following flash chromatography (15% ethyl acetate in petroleum ether) the resultant solvent was evaporated to give pure **25** (73% yield). ^{1}H NMR (400 MHz, $CDCl_3$) δ: 11.23 (broad s, 1H), 3.12-3.18 (dd, 5.31 Hz, 5.50 Hz, 1H), 2.99-3.06 (dd, 8.61 Hz, 8.79 Hz, 1H), 2.58-2.71 (m, 1H), 2.34 (s, 3H), 1.52-1.76 (m, 2H), 1.28-1.42 (m, 4H), 0.91 (t, 7.05 Hz, 3H). ^{13}C NMR (100 MHz, $CDCl_3$) δ: 195.7, 180.6, 45.7, 31.5, 31.0, 29.9, 29.7, 22.7, 14.4.

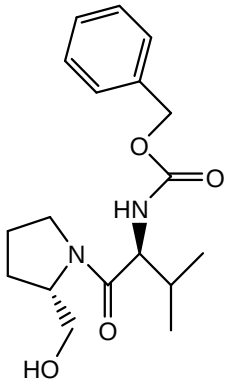

***N*-Benzyloxycarbonyl-L-valyl-L-prolinol (9)**. [15] $C_{18}H_{26}N_2O_4$. Z-Valine-*O*-nitrophenyl ester (**8**) (5.45 g, 14.63 mmol) was dissolved in ethyl acetate (25 mL) and placed under N_2. Next, L-prolinol (**7**) (1.43 mL, 14.63 mmol) was added to the reaction mixture, which was allowed to stir for 48 hrs. Then, chloroform (20 mL) was added and washed with 2N HCl (20 mL). Next, it was washed with 2N NH_4OH (3 x 20 mL portions) and H_2O (30 mL). The organic layer was dried with $MgSO_4$ and the solvent evaporated to give **9** (99% yield). ^{1}H NMR (400 MHz, $CDCl_3$) δ: 7.28-7.38 (m, 5H), 5.59 (d, 8.97 Hz, 1H), 5.00-5.14 (m, 2H), 4.22-4.46 (m, 4H), 3.80-3.89 (m, 1H), 3.45-3.71 (m, 3H), 1.81-2.10 (m, 4H), 1.55-1.64 (m, 1H), 1.03 (d, 6.78 Hz, 3H), 0.96 (d, 6.78 Hz, 3H). ^{13}C NMR (100 MHz, $CDCl_3$) δ: 173.3, 156.7, 136.5, 128.7, 128.3, 128.2, 67.2, 67.1, 58.0, 48.5, 31.7, 28.2, 24.7, 19.5, 17.8.

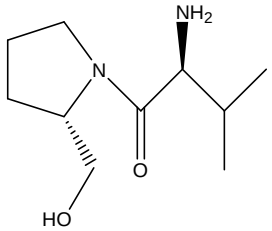

L-Valyl-L-prolinol (2). *N*-Benzyloxycarbonyl-L-valyl-L-prolinol (**9**) (3.308 g, 9.892 mmol) was dissolved in ethyl acetate (200 mL) and placed in a bomb hydrogenator with Pd/C (10% wt., 300 mg) under H_2 (425 psi) for 2 days. Filtered with Celite and flash chromatography (5% MeOH/95% CH_2Cl_2/0.5% NH_4OH) gave product **2** (96% yield). ^{1}H NMR (400 MHz, $CDCl_3$) δ: 4.21-4.28 (m, 1H), 3.39-3.62 (m, 5H), 3.11 (d, 5.86 Hz, 1H), 2.44-2.54 (m, 1H), 1.70-2.40 (m, 4H), 1.52-1.60 (m, 1H), 0.975 (d, 6.23 Hz, 3H), 0.925 (s, 3H). ^{13}C NMR (100 MHz, $CDCl_3$) δ: 176.8, 67.3, 62.7, 60.9, 47.9, 31.7, 27.9,

24.0, 19.5, 18.3. +EI-GC-MS showed one predominant peak with a retention time of 10.41 minutes and 97% purity. The parent ion weight observed was 201 amu(100) (desired product plus H^+).

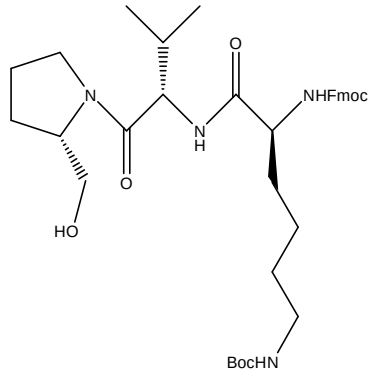

***N*^{2}-Fluorenylmethoxycarbonyl-L-(*N*^{6}-Boc)-L-valyl-L-prolinol (31)**. $C_{36}H_{50}N_4O_7$. L-valyl-L-prolinol (**2**) (2.048 g, 10.21 mmol) was dissolved in CH_2Cl_2 (80 mL). Next, Fmoc-Lys(Boc)-OH (**32**) (4.784 g, 10.21 mmol) was added along with DCC (2.107 g, 10.21 mmol) all under N_2 at room temperature. The solution was allowed to mix overnight. Flash chromatography (3% MeOH/97% CH_2Cl_2) in a large column yielded product **31** (82% yield). ^{1}H NMR (400 MHz, d_6-acetone) δ: 7.85 (d, 7.51 Hz, 2H), 7.71 (t, 7.60 Hz, 2H), 7.42-7.52 (m, 1H), 7.41 (t, 7.50 Hz, 2H), 7.32 (t, 7.51 Hz, 2H), 4.52-4.71 (m, 1H), 4.21-4.37 (m, 4H), 4.10-4.18 (m, 1H), 3.68-3.87 (m, 1H), 3.40-3.64 (m, 3H), 2.98-3.12 (m, 2H), 2.88 (s, 3H), 1.64-2.09 (m, 11H), 1.39 (s, 9H), 0.93 (m, 6H). ^{13}C NMR (100 MHz, d_6-DMSO, 50 °C) δ: 173.1, 157.1, 145.1, 144.9, 142.1, 128.6, 128.0, 126.2, 120.8, 78.3, 67.3, 65.1, 63.2, 56.4, 55.2, 48.1, 48.0, 47.9, 40.7, 32.1, 32.0, 28.8, 27.8, 25.2, 24.5, 23.8, 23.0, 20.3, 18.1.

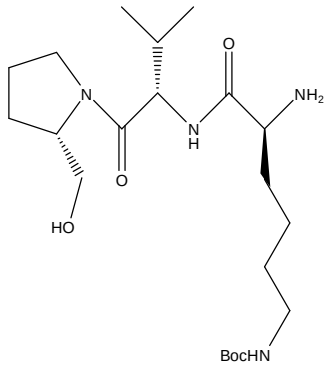

L-(N^6-Boc)-L-valyl-L-prolinol (32). $C_{21}H_{40}N_4O_5$. N^2-Fluorenylmethoxycarbonyl-L-(N^6-Boc)-L-valyl-L-prolinol (**31**) (1.00 g, 1.54 mmol) was dissolved in DMF (4.79 mL, 4.50 g) and DMAP (0.50 g, 4.1 mmol) was added all under N_2 at room temperature. After 48 hrs., flash chromatography in a large silica column (flushed with 3 L petroleum ether, then used 3%MeOH/97% CH_2Cl_2/few drops NH_4OH) was employed to yield product **32** in low yield (30%). The purification was done for the purposes of NMR studies; subsequent reaction attempts just carried the crude material on to the next step along with excess DMAP without any flash chromatography. Qualitatively, the ^1H NMR spectra showed the absence of the Fmoc protons and carbons. ^1H NMR (400 MHz, d_6-acetone) δ: 4.28-4.71 (m, 4H), 4.06-4.21 (m, 2H), 3.85-3.90 (m, 1H), 3.72-3.82 (m, 1H), 3.35-3.70 (m, 4H), 2.98-3.12 (m, 2H), 1.62-2.08 (m, 11H), 1.39 (s, 9H), 0.88-0.98 (m, 6H). ^{13}C NMR (100 MHz, d_6-acetone) δ: 173.8, 172.5, 157.1, 78.7, 65.1, 61.2, 56.1, 56.0, 48.7, 41.4, 32.7, 31.4, 29.1, 28.4, 25.4, 24.1, 22.6, 20.4, 18.5.

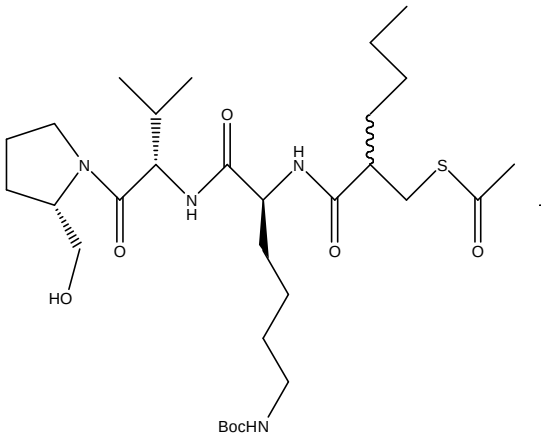

L-N^2-(3-Acetyl mercapto-2-butylpropionyl)-(N^6-Boc)-L-valyl-L-prolinol (33). $C_{30}H_{54}N_4O_7S$. L-(N^6-Boc)-L-valyl-L-prolinol (**32**) (1.648 g, 3.850 mmol) was dissolved

in CH_2Cl_2 (30 mL) and 3-acetylmercapto-2-butylpropionic acid (**25**) (0.7854 g, 3.850 mmol) and DCC (0.7944 g, 3.850 mmol) were added. The reaction mixture was placed under N_2 at room temperature. Flash chromatography (1 L diethyl ether flush, then 2% MeOH/98% CH_2Cl_2/NH_4OH in large silica column) produced product **33** (58% over 3 steps). ^{1}H NMR (400 MHz, d_6-DMSO, 50°C) δ: 3.79-4.72 (m, 6H), 3.30-3.52 (m, 3H), 3.02-3.22 (m, 3H), 2.69-2.90 (m, 6H), 2.27-2.55 (m, 3H), 2.20 (s, 3H), 1.60-1.93 (m, 6H), 1.32-1.59 (m, 4H), 1.28 (s, 9H), 1.04-1.19 (m, 5H), 0.68-0.81 (m, 6H). ^{13}C NMR (100 MHz, d_6-DMSO, 50 °C) δ: 173.0, 171.2, 169.6, 155.4, 77.2, 61.1, 58.4, 55.5, 46.8, 45.2, 40.2, 31.7, 31.5, 30.8, 30.3, 29.0, 28.5, 28.1, 23.5, 22.5, 21.9, 21.8, 18.9, 17.8, 13.5. +ESI-MS showed 615 amu (100) (desired product plus H^+).

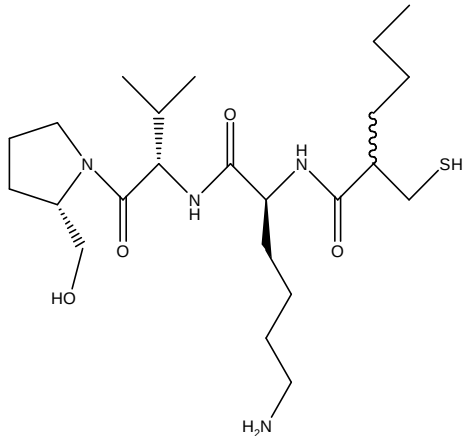

Thiol-Actinonin Chimera (34a + b). $C_{23}H_{44}N_4O_4S$. L-N^2-(3-Acetyl mercapto-2-butylpropionyl)-(N^6-Boc)-L-valyl-L-prolinol (**33**) (960 mg, 1.56 mmol) was dissolved in dry EtOH (25 mL) in a Schlenk flask under N_2. Then, $NaBH_4$ (500 mg, 12.5 mmol) was added and the reaction mixed for ~24 hrs. Next, H_2O (3 mL) and 5% HCl (1 mL) were added to quench the reaction. The volatile solvents were evaporated and the residue was dissolved in ethyl acetate (20 mL). This solution was washed with sat. NaCl (2 x 20 mL), the organic layer was dried via $MgSO_4$, and the resultant solvent evaporated. This product was carried directly over to the next step, which entailed dissolving the reaction mixture in CH_2Cl_2 (45 mL) and then adding TFA (6.52 mL, 87.7 mmol) and allowing to stir overnight under N_2. Flash chromatography (initially used 3% MeOH/ 97% CH_2Cl_2/NH_4OH and gradually increased the volume of MeOH) and RP-HPLC (50-min acetonitrile gradient (0-100%) in 0.1 % TFA aqueous solution; 28.49 min R_t for diast. 1,

and R_t 29.46 min. for diast. 2) yielded the product diastereomers **34a** + **34b**. ^{1}H NMR (400 MHz, d_6-DMSO, 50 °C) δ: 7.98-8.13 (m, 1H), 7.45-7.78 (m, 3H), 5.20-6.25 (broad m, 6H), 4.15-4.69 (m, 2H), 3.73-4.03 (m, 1H), 3.42-3.67 (m, 1H), 3.18-3.35 (m, 1H), 2.38-2.80 (m, 6H), 1.62-2.20 (m, 6H), 1.14-1.60 (m, 7H), 0.78-0.93 (m, 6H). ^{13}C NMR (100 MHz, d_6-DMSO, 50 °C)
δ: 174.2, 172.1, 170.5, 61.8, 59.2, 56.3, 55.2, 53.0, 50.0, 41.0, 32.2, 31.9, 31.5, 31.0, 29.6 , 29.4, 27.1, 22.9, 22.6, 19.7, 18.7, 14.4. +EI-MS showed the highest molecular ion to be 473 amu (desired product plus H^+).

Chapter 4: Biological Analysis of Pei's Inhibitor 29b and the Chimera 34

The following subsections deal with the leaf-painting experiments, seed germination tests, and the enzyme assays performed on the chimera **34**. Also, the following subsections deal with the leaf-painting experiments and seed-germination tests on Pei's thiol inhibitor **29b**. No enzyme assays were performed with Pei's thiol inhibitor **29b**. The preliminary results show the thiol-actinonin chimera to be an inhibitor of *At*DEF2 and a comparison of it's potency to actinonin **1** and Pei's inhibitor **29b** it was mimicked off of is given.

4.1 Seed Germination Analysis

Seed germination analysis was conducted on the two thiol inhibitors, Pei's **29b** and the thiol-actinonin chimera **34**. At the time of this experimentation, this batch of **34** inhibitor had NOT undergone RP-HPLC purification; it was still crude. The growth medium for this experiment was comprised of a Murashige and Skoog salt mixture, agar, 100 X MES buffer solution (pH 5.6), and H_2O. This growth medium was applied to the test plates while still in viscous gel phase. The seeds used were either wild type (WT) or pdf over-expressor (OE) tobacco seeds; both of which were sterilized prior to testing.

For **34**, a 100 mM stock solution was made from which 20 μL (= 5mM final concentration) was injected into 380 μL of growth medium in 18 test plate wells. The first lane of six wells was OE seeds, while the second lane consisted of WT seeds, and the third lane of six wells possessed WT seeds with no inhibitor. The result from this seed germination test after 4 days was the OE seeds showed initial stages of cotyledon growth, the WT-inhibitor seeds showed radical emergence, and the WT-no inhibitor showed normal cotyledon growth. This seemed promising at first, especially considering that the imhibitor material was crude, but after a week to 10 days most of the wells showed medium to full cotyledon development (data not shown due to preliminary experimentation with crude material; needs further tests). It could be inferred that the inhibitor was somehow metabolized by the proteolytic enzymes found in vivo, but it is hard to be certain when the material was crude. This experiment will be repeated with the latest batch of purer chimera inhibitor diastereomers **34**.

Pei's inhibitor **29b** was also made into a 100 mM stock solution from which 20 μL (= 5mM final concentration) was injected into 380 μL of growth medium in 30 wells of the test plate. The first two lanes (12 wells) contained a tobacco WT seed. The next lane and a third (8 wells) contained tobacco OE seeds. The final lane (6 wells) contained WT seeds with no inhibitor. The result of this seed germination test after 4 days-12 days showed the complete inhibition of growth past radicale emergence (data not shown due to preliminary experimentation; needs further tests).

4.2 Leaf-Painting Analysis

Leaf-painting analysis required making 10 mg/ mL solutions + 0.1% (v/v) Tween 20 (a detergent from Sigma, which helps the inhibitor cross the membrane) of each inhibitor and applying 300 μL of the solution to the leaves of the plants over 6 days. An additional solution was made for **29b** due to the difficulty of dissolving the inhibitor in an aqueous solution. This solution contained the usual 10 mg/mL of inhibitor as well as the 0.1% Tween 20, but also contained 0.5% acetone to help the inhibitor dissolve more quickly and efficiently. Again, it is important to note that the same batch of inhibitor **34** that was used in the seed germination tests was also used in this line of experimentation, meaning that it was crude.

The application of **34** to tobacco leafs in 300 μL + 0.1% Tween 20 portions daily. The result of this experiment was the initial signs of bleaching of color after 1-2 days. However, the bleaching that was observed quickly disappeared, and the experiment failed to kill the plants (data not shown). This may be attributed to the inhibitor being degraded by enzymes in vivo, or it might be related to a lower dose of the inhibitor actually being used due to the crude nature of the material.

The two **29b** solutions, one with 0.5% acetone and one without the acetone, were applied to 2 tobacco plants each. Additionally, 1 pea plant that possessed two sets of true leaves was treated with **29b**, as well as 1 small pea plant without true leaves. After daily applications of 300 μL of the inhibitor + 0.1% of Tween 20 solution, the result was a stronger and more intense bleaching effect of the leaves than seen with **34**. However, the bleaching soon disappeared and the plants grew normally. This would indicate that the plant may be metabolizing the thiol inhibitor **29b** just as it did with actinonin (**1**). More inhibitor would have to be synthesized and the experiments run again in conjunction with

the new **34** experiments in order to clearly understand the implications of the aforementioned outcome.

4.3 Enzyme Assays of 34a and 34b

Spectrophotometric enzyme assays[23,47] of *At*DEF2 activity were conducted at room temperature (25 °C) with a pH 8 buffer solution containing 0.1 mM $NiSO_4$, methionine aminopeptidase (MAP, 1U/ μL) and using the thiol inhibitor diastereomers **34a** and **34b** (new batch, post RP-HPLC) and the enzyme substrate *N*-formyl-Met-Leu-*p*-nitroaniline (f-ML-*p*NA). The release of the conjugated *p*-nitroaniline group was measured by monitoring the absorbance increase at 405 nm. The data was charted on the instrument computer as milli-Absorbance per minute (mAbs./min) in order of decreasing activity with increasing inhibitor concentration. The results for **34a** and **34b** + byproduct are tabulated in Tables 4.1 and 4.2, respectively, and figures 4.1 and 4.2 respectively.

Table 4.1: 34a's Effect on *At*DEF2's (Ni) Activity. For each assay, 0.62 μL of 1/10 Ni-*At*DEF2 was used.

Run #	**Inhibitor (conc. x volume = moles)**	**Slope (mAbs/min)**
1	100 μM 100 μL = 10000 nM	37.88
2	100 μM 80 μL = 8000 nM	118.8
3	100 μM 60 μL = 6000 nM	276.5
4	100 μM 40 μL = 4000 nM	526.5
5	100 μM 30 μL = 3000 nM	640.5
6	100 μM 15 μL = 1500 nM	652.5
7	100 μM 5 μL = 500 nM	693.0
Blank	No Inhibitor	801.9

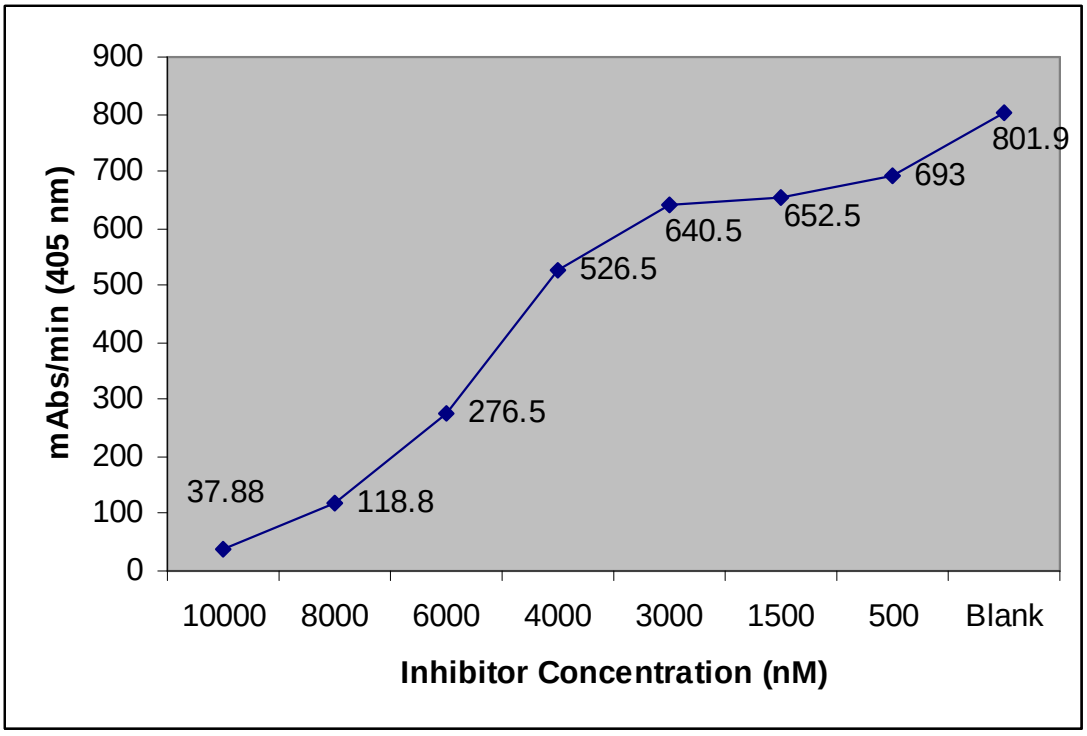

Figure 4.1: 34a: Inhbition of *At*DEF2 (Ni) Activity.

The minimum inhibitory concentration (MIC) of **34a** seen in Table 4.1 and Figure 4.1 is 500 nM. The 50% inhibitory concentration (IC_{50}) of **34a** is 5000 nM.

Table 4.2: 34b + Byproduct's Effect on *At*DEF2's (Ni) Activity. For each assay, 0.62 μL of 1/10 Ni-*At*DEF2 was used.

Run #	**Inhibitor (conc. x volume = moles)**	**Slope (mAbs/min)**
1	100 μM 100 μL = 10000 nM	5.98
2	100 μM 60 μL = 6000 nM	78.11
3	100 μM 30 μL = 3000 nM	201.0
4	100 μM 15 μL = 1500 nM	326.7
5	100 μM 5 μL = 500 nM	451.1
6	100 μM 2 μL = 200 nM	587.0
Blank	No Inhibitor	801.9

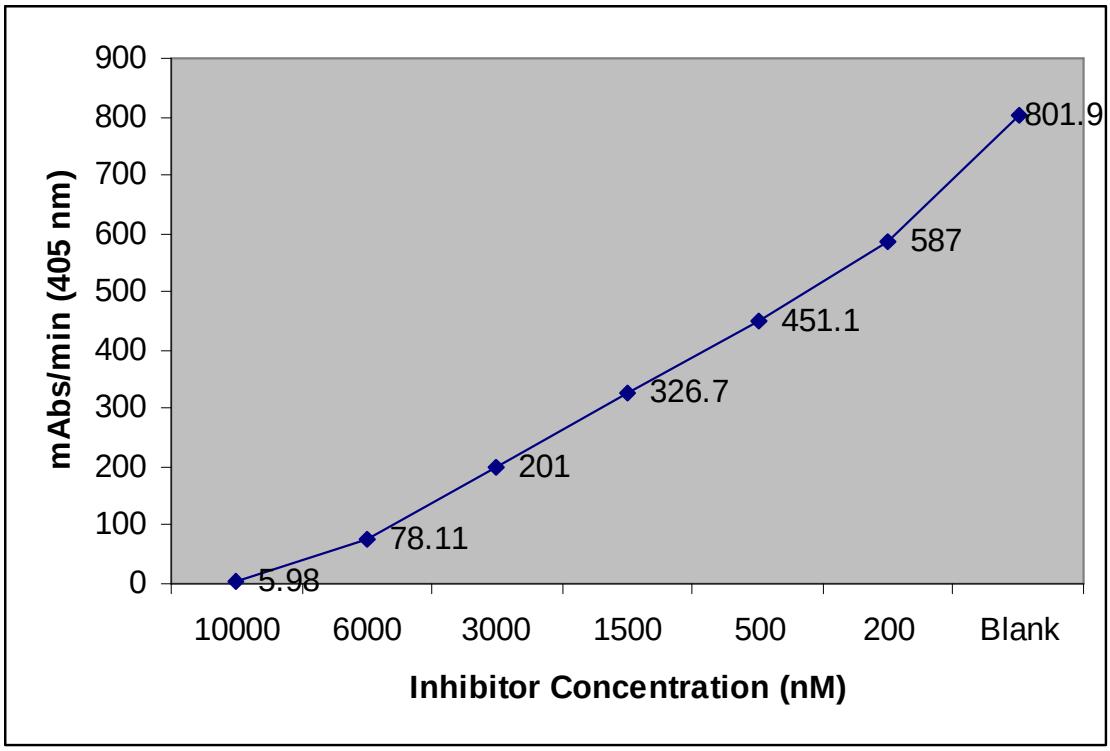

Figure 4.2: 34b + Byproduct: Inhbition of *At*DEF2 (Ni) Activity.

The minimum inhibitory concentration (MIC) of **34b + byproduct** seen in Table 4.2 and Figure 4.2 is 200 nM. The 50% inhibitory concentration (IC_{50}) of **34b = byproduct** is 1000 nM.

Table 4.3: Comparison of the MIC and IC_{50} between Actinonin 1, Pei's Thiol 29b, and the Thiol-Actinonin Chimera 34a + b. Values are from literature or from experimentation discussed above.[20, 23, 32]

	MIC	IC_{50}
Actinonin **1** (*E coli* Ni-PDF)	25.0 nM	3.0 nM
Pei's Thiol **29b** (*E. coli*: Ni-PDF)	75-100 μM	N/A
Chimera **34a** (*At*DEF2: Ni-PDF)	500 nM	5000 nM
Chimera **34b + byproduct** (*At*DEF2: Ni-PDF)	200 nM	1000 nM

Table 4.3 shows the MIC and IC_{50} values for each of the inhibitors discussed throughout this thesis. It is important to first point out that the enzyme assays conducted to obtain the data above were done with *E. coli* for **1** and **29b** and with *At*DEF2 for **34a** and **34b+byproduct**. Actinonin is the most potent of the group with an MIC of 25.0 nM and an IC_{50} of 3.0 nM for *E. coli* Ni-PDF. Compare that with the other extreme, Pei's thiol **29b**, and it is evident the loss in potency is 3000 to 4000-fold. However, it is interesting to point out that the chimeras **34a** and **34b+byproduct** show a much higher potency than **29b** by 150 to 250-fold and 375 to 500-fold, respectively. One is able to extrapolate from the data presented in Table 4.3, even when considering the differing hosts, the effect of changing the hydroxamate group on actinonin **1** to a sulfhydryl group to make the chimera **34**. The chimera **34a** is 20 times less potent during in vitro enzyme assays than actinonin and **34b + byproduct** is only 8 times less potent. It would be interesting to do the same *Arabidopsis thaliana* assays with **29b** to see what the MIC and IC_{50} are. Dirk et al.[23] did the *At*DEF2 assay with actinonin and observed an IC_{50} at 50-100 nM, which is even closer in potency to the data for **34a** and **34b + byproduct**.

Therefore, we have shown that the thiol-actinonin chimera **34a or b** is truly a hybrid that favors more closely the characteristic potency observed with actinonin **1** than with Pei's thiol inhibitor **29b**.

Even though **34b** has an equal amount of byproduct present, it still did not show any substantial potency difference from the much more pure diastereomer **34a**. Hence, the two were kept together for the purposes of NMR and MS data experiments. The next enzyme assay should involve the use of a mixture of the diastereomers since they have the same activity.

Methionine aminopeptidase assays were also conducted to determine if the inhibitor had any effect on the particular enzyme using a different substrate (no *N*-formyl, rather start with methionine). At high, or low, concentrations of **34**, 6000nM and 1000 nM of either diastereomer, the enzyme methionine aminopeptidase showed high activity as evidenced by the 8382 and 9291 mAbs/min slope, respectively. Therefore, the inhibitor diastereomers **34a+b** were not a factor in MAP inhibition.

4.4 Experimental Section

Seed Germination Tests.

I imbibed Tobacco seeds (wild type [WT] and over expresser [OE]) and the seedlings were cultured at room temperature with constant light (50 μmol $m^{-2}s^{-1}$) in a 1% agar/380 μl Murashige and Skoog basal salts (Sigma) medium in the wells of a 96-well microtiter. The cultures were done either in the absence or presence of either of the thiol inhibitors, **29b** and **34**.

Leaf-Painting Analysis.

10 mg/ml + 0.1% Tween 20 aqueous solutions of both thiol inhibitors were comprised. These solution mixtures were then applied to tobacco and pea plants of various maturity and growth in 300 μL volumes on a daily basis. Observations were made visually based on discoloration and bleaching.

Enzyme Assays.

Spectrophotometric assays of *At*DEF2 activity[23,47] were conducted at 25 °C in polystyrene cuvettes containing 885-985 μL of pH 8 buffer with 0.1 mM $NiSO_4$, with 1 unit of *Aeromonas proteolytica* methionine aminopeptidase (MAP, 1U/ μL; Sigma, St. Louis) and 2-100 μL of 100 μM of thiol inhibitor diastereomers **34a+b** (new batch, post

RP-HPLC) and 10 μL of 20 mM of the enzyme substrate *N*-formyl-Met-Leu-*p*-nitroaniline (f-ML-*p*NA substrate was the initiator of the assay, BACHEM Bioscience Inc., King of Prussia, PA). The release of *p*-nitroaniline was measured by monitoring the increase in absorbance at 405 nm using a UV-201 PC scanning spectrophotometer (Shimadzu Scientific Instruments, Inc., Columbia, MD).

Chapter 5: Conclusion

The enzyme peptide deformylase (PDF) is responsible for the removal of the formyl group located at the N-terminus of nascent proteins in order for them to become mature, functioning proteins. It exists in prokaryotic and eukaryotic forms, in bacteria, chloroplasts, and mitochondria. However, only in bacteria and plants has it been shown that proteins require the removal of the formyl group post-translation in order to function properly. PDF has been studied extensively, as evidenced by the vast number of articles published yearly on the subject, and has been shown to be a mononuclear metalloprotease. Because metalloproteases are so widely studied and are the best-known form of enzymes, PDF is a target for the antibiotics and herbicidal industry. It has even been proposed to be viable for use as a selectable marker. A selectable marker is a genetically engineered reporter gene that indicates whether or not a successful transfer of foreign DNA into a cell was made by growing the target in an environment laden with PDF inhibitor. The colonies that survive the inhibitor medium have taken up and expressed the injected foreign DNA.

Over the past 4 decades, many scientists have tried to design and synthesize inhibitors of PDF in order to create the next new antibiotic, or herbicide. The best naturally known in vitro inhibitor of PDF is actinonin. The biggest problems with actinonin are that it is too expensive to purchase on a massive scale, and it is too easily metabolized in vivo. Therefore, several attempts at making analogues of the hydroxamate inhibitor have been made, to not much avail. The next generation of inhibitors specifically designed to inhibit PDF was created by Dr. Pei at Ohio State University. These inhibitors showed potency, but eventually experienced a similar in vivo problem as actinonin. The compound I designed and synthesized seems to suffer from the same drawback. There still needs to be work done in order to solidify this preliminary observation. The last generation of inhibitors, the macrocyclic reverse-hydroxamate inhibitors also created by Dr. Pei, seem to be working well as far as potency and in vivo survival are concerned. However, as of this date, there are no articles describing the ability of these macrocyclic inhibitors to inhibit plant PDF. It would be interesting to determine the efficacy of the macrocyclic inhibitors.

There were many goals to be accomplished and that were accomplished throughout the course of my research. The first goal consisted of modeling and analyzing the three different types of active sites of PDF; *At*DEF1, *At*DEF2, and *Ecoli*DEF2. Most importantly for the scope of my project was the *At*DEF2 due to its location in the thylakoid membrane of chloroplasts and its 100-fold higher activity than *At*DEF1. In the midst of the analysis of the different active sites, several residues were found to be fairly consistently different between *At*DEF1 and 2 and between *At*DEF2 and *Ecoli*DEF2. This is important because in order for a designed inhibitor to be selective towards plant PDF versus bacterial PDF, there must exist a difference between the types of PDF; more specifically between *At*DEF2 and *Ecoli*DEF2. With the further work soon to be accomplished on the molecular dynamics front, we should have a better idea just how important those differing residues really are and how well the *At*DEF2 preferred D1 substrate binds to the active site and why it is not preferred by *At*DEF1.

The second goal was to synthesize a peptide-based thiol inhibitor designed by Pei and synthesize one that mimicked actinonin **1** in regards to the backbone and a sulfhydryl in regards to the chelating portion of the compound. Both of these synthetic goals were accomplished, and the purity of the resulting chimera is the best it's ever been. It is good enough right now to run new leaf-painting analyses and seed germination tests to see how potent the diastereomeric mixture of the inhibitor **34** truly is. The enzyme assays showed that it does in fact inhibit *At*DEF2, albeit not as intensely as actinonin, but close. It was more potent than Pei's thiol **29b** and upon further experiments, might survive in vivo tests where actinonin failed. It is difficult to conclude at this juncture if the chimera **34** is being metabolized based on the crude material that was used to conduct the analyses.

In closing, we have found many consistent differences between the three types of PDF enzymes, synthesized a novel thiol-actinonin chimera **34**, begun new syntheses of D1 substrate mimics, and tested the biological efficacy of said inhibitors in crude form, and will retest the more pure form of each to determine the true PDF inhibitory prowess they may possess.

References

1) Adams, J.M. *J. Mol. Biol.* **1968**, *33*, 571-589.

2) Sherman, F.; Stewart, J.W., Tsunasawa, S. *BioEssays* **1985**, *3*, 27-31.

3) Rajagopalan, P.T.R.; Pei, D. *J. Biol. Chem*. **1998**, *273*, 22305-22310.

4) Meinnel, T.; Blanquet, S. *J. Bacteriol.* **1993**, *175*, 7737-7740.

5) Meinnel, T.; Blanquet, S. *J. Bacteriol.* **1995**, *177*, 1883-1887.

6) Rajagopalan, P.T.R.; Datta, A.; Pei, D. *Biochemistry* **1997**, *36*, 13910 – 13918.

7) Groche, D., *Thesis, Universität Heidelberg, Germany*. **1995**.

8) Groche, D.; Wagner, A.F.V. *15th Conference of the GDCh Fachgruppe Biochemie, Giessen.* 1996, Abstract No. 58.

9) Groche, D.; Becker, A.; Schlichting, E.; Kabasch, W.; Schultz, S.; Wagner, A.F.V. *Biochem. Biophys. Res. Commun*. **1998**, *246*, 342-346.

10) Meinnel, T.; Lazennec, C.; Villoing, S.; Blanquet, S. *J. Mol. Biol.* **1997**, *267*, 749-761.

11) Becker, A.; Schlichting, I.; Kabasch, W.; Groche, D.; Schultz, S.; Wagner, A.F.V., *Nat. Struct. Biol*. **1998**, *5*, 1053-1058.

12) Gordon, J.J.; Kelly, B.K.; Miller, G.A. *Nature* **1962**, *195*, 701.

13) Gordon, J.J.; Devlin, J.P.; East, A.J.; Ollis, W.D.; Sutherland, I.O.; Wright, D.E.; Ninet, L. *J. Chem. Soc., Perkin Trans*. **1975**, *1*, 819.

14) Bentley, R. '*Molecular Asymmetry in Biology,*' Academic Press, New York **1969**, *1*, 239.

15) Anderson, N.H.; Ollis, W.D.; Thorpe, J.E.; Ward, A.D. *J. Chem. Soc., Perkin Trans.* **1975**, *1*, 825.

16) Devlin, J.P.; Ollis, W.D.; Thorpe, J.E.; Wood, R.J.; Broughton, B.J.; Warren, P.J.; Wooldridge, K.R.H.; Wright, D.E. *J. Chem. Soc., Perkin Trans*. **1975**, *1*, 830.

17) Broughton, B.J.; Warren, P.J.; Wooldridge, K.R.H.; Wright, D.E.; Ollis, W.D.; Wood, R.J. *J. Chem. Soc., Perkin Trans*. **1975**, *1*, 842.

18) Devlin, J.P.; Ollis, W.D.; Thorpe, J.E. *J. Chem. Soc., Perkin Trans*. **1975**, *1*, 846.

19) Devlin, J.P.; Ollis, W.D.; Thorpe, J.E.; Wright, D.E. *J. Chem. Soc., Perkin Trans.* **1975**, *1*, 848.

20) Chen, D.Z.; Patel, D.V.; Hackbarth, C.J.; Wang, W.; Dreyer, G.; Young, D.J.; Margolis, P.S.; Wu, C.; Ni, Z.J.; Trias, J.; White, R.J.; Yuan, Z. *Biochemistry* **2000**, *39*, 1256-1262.

21) Hanson, A.D.; Gage, D.A.; Shachar-Hill, Y. *Trends Plant Sci*. **2000**, *5*, 206-213.

22) Williams, M.A.; Dirk, L.M.A.; Houtz, R.L. *Plant Physiology* **2000**, *123*, S-131.

23) Dirk, L.M.A.; Williams, M.A.; Houtz, R.L. *Plant Physiology* **2001**, *127*, 97-107.

24) Dirk, L.M.A.; Williams, M.A.; Houtz, R.L. *Archives of Biochemistry and Biophysics* **2002**, *406*, 135-141.

25) Hou, C.X.; Dirk, L.M.A.; Williams, M.A. *American J. of Botany* **2004**, *91*(9), 1304-1311.

26) Hou, C.X.; Dirk, L.M.A.; Goodman, J.P.; Williams, M.A. *Weed Science* **2006**, *54*, 246-254.

27) Apfel, C.; Banner, D.W.; Bur, D.; Dietz, M.; Hirata, T.; Hubschwerlen, C.; Locher, H.; Page, M.G.P.; Pirson, W.; Rosse, G.; Specklin, J.L. *J. Med. Chem*. **2000**, *43*, 2324-2331.

28) Jayasekera, M.M.K.; Kendall, A.; Shammas, R.; Dermyer, M.; Tomala, M.; Shapiro, M.A.; Holler, T.P. *Arch. Biochem. Biophys*. **2000**, *381*, 313-316.

29) Thorarensen, A.; Douglas, M.R.,Jr.; Rohrer, D.C. et al. *Bioorg. Med. Chem. Lett*. **2001**, *11*, 1355-1358.

30) Roblin, P.M.; Hammerschlag, M.R. *Antimicrob. Agents Chemother*. **2003**, *47*, 1447-1448.

31) Meinnel, T.; Patiny, L.; Ragusa, S.; Blanquet, S. *Biochemistry* **1999**, *38*, 4287-4295.

32) Huntington, K.M.; Yi, T.; Wei, Y.; Pei, D. *Biochemistry* **2000**, *39*, 4543-4551.

33) Wei, Y.; Yi, T.; Huntington, K.M.; Chaudhury, C.; Pei, D. *J. Comb. Chem*. **2000**, *2*, 650-657.

34) Hu, X.; Ngyuen, K.T.; Verlinde, C.L.M.J.; Hol, W.G.J.; Pei, D. *J. Med. Chem.* **2003**, *46*, 3771-3774.

35) Hu, X.; Ngyuen, K.T.; Jiang, V.C.; Lofland, D.; Moser, H.E.; Pei, D. *J. Med. Chem.* **2004**, *47*, 4941-4949.

36) Xue, C.B.; He, X.; Roderick, J. et al. *J. Med. Chem*. **1998**, *41*, 1745-1748.

37) Wei, C.Q.; Gao, Y.; Lee, K. et al. *J. Med. Chem*. **2003**, *46*, 244-254.

38) Lazennec, C.; Meinnel, T.; *Anal. Biochem.* **1997**, *244*, 180-182.

39) Clements, J.M.; Beckett, R.P.; Brown, A.; Catlin, G.; Lobell, M.; Palan, S.; Thomas, W.; Whittaker, M.; Wood, S.; Salama, S.; baker, P.J.; Rodgers, H.F.; Barynin, V.; Rice, D.W.; Hunter, M.G. *Antimicrob. Agents Chemother*. **2001**, *45*, 563-570.

40) *Research Collaboratory for Structural Bioinformatics PDB*, URL http://www.rcsb.org/pdb/.

41) PDB ID: 1BS5.
Becker, A.; Schlichting, I.; Kabsch, W.; Groche, D.; Schultz, S.; Wagner, A.F. *Nat. Struct. Biol.* **1998**, *5*, 1053-1058.

42) PDB ID: 1ZXZ.
Fieulaine, S.; Juillan-Binard, C.; Serero, A.; Dardel, F.; Giglione, C.; Meinnel, T.; Ferrer, J.-L. *To be Published.*

43) *Basic Local Alignment Search Tool (BLAST)*, URL http://www.ncbi.nlm.nih.gov/BLAST/.

44) *TargetP 1.1 Server*, URL http://www.cbs.dtu.dk/services/TargetP

45) *Multiple Sequence Alignment by CLUSTALW*, URL http://clustalw.genome.jp/.

46) PDB ID: 1BS8
Becker, A.; Schlichting, I.; Kabsch, W.; Groche, D.; Schultz, S.; Wagner, A.F. *Nat.Struct.Biol.* **1998**, *5*, 1053-1058.

47) Wei, Y.; Pei, D. *Analytical Biochemistry* **1997**, *250*, 29-34.

Vita

The author was born on January 13, 1982 in Louisville, Kentucky. Jonathan arrived at the University of Kentucky in the Fall of 2000 as an undergraduate and entered the University Scholars Program in the Spring of 2005. He did his undergraduate research with Dr. Robert B. Grossman and subsequently decided to join Dr. Grossman's research group to achieve his Master's degree. As an undergraduate, Jonathan received the Thomas B. Nantz Excellence in Chemistry Scholarship Award (2002-2004) and maintained a Summa Cum Laude accreditation as an undergraduate and a graduate student.